molecules

MDPI

Review

Recent Advance in Co_3O_4 and Co_3O_4-Containing Electrode Materials for High-Performance Supercapacitors

Xuelei Wang [1,2], Anyu Hu [1], Chao Meng [1], Chun Wu [1], Shaobin Yang [1,2] and Xiaodong Hong [1,*]

[1] College of Materials Science and Engineering, Liaoning Technical University, Fuxin 123000, China; wangxuelei-19@163.com (X.W.); huanyu990428@163.com (A.H.); mikko_mc@163.com (C.M.); chun_wu@126.com (C.W.); lgdysb@163.com (S.Y.)

[2] College of Mining, Liaoning Technical University, Fuxin 123000, China

* Correspondence: hongxiaodong@lntu.edu.cn; Tel.: +86-0418-511-0099

Received: 28 November 2019; Accepted: 6 January 2020; Published: 9 January 2020

Abstract: Among the popular electrochemical energy storage devices, supercapacitors (SCs) have attracted much attention due to their long cycle life, fast charge and discharge, safety, and reliability. Transition metal oxides are one of the most widely used electrode materials in SCs because of the high specific capacitance. Among various transition metal oxides, Co_3O_4 and related composites are widely reported in SCs electrodes. In this review, we introduce the synthetic methods of Co_3O_4, including the hydrothermal/solvothermal method, sol–gel method, thermal decomposition, chemical precipitation, electrodeposition, chemical bath deposition, and the template method. The recent progress of Co_3O_4-containing electrode materials is summarized in detail, involving Co_3O_4/carbon, Co_3O_4/conducting polymer, and Co_3O_4/metal compound composites. Finally, the current challenges and outlook of Co_3O_4 and Co_3O_4-containing composites are put forward.

Keywords: Co_3O_4; supercapacitor; composite; electrode material

1. Introduction

Energy crisis and environmental pollution trigger the development of energy storage systems toward clean and renewable energies. Supercapacitors (SCs) act as a new type of energy storage devices between conventional capacitors and batteries [1]. The energy stored and released amount are related to the speed in energy storage devices [2]. In general, the greater the discharge power, the lower the energy that can be released [3]. The performance of SCs mainly involves specific capacitance (Cs), specific energy (E), specific power (P), resistance, cycling stability, and rate capacity. These are obtained by electrochemical cyclic voltammetry (CV), galvanostatic charge/discharge (GCD), and electrochemical impedance spectroscopy (EIS) [4]. The E of SCs is several hundred times higher than that of traditional capacitors, and the P is two orders of magnitude higher than that of the batteries. SCs make up the shortcomings of low specific power, poor charge, and discharge performance of large currents and low specific energy of conventional capacitors.

The above performances are closely related to the working principle of SCs. Based on the working principle, SCs involve electric double layer capacitors (EDLCs) and pseudocapacitors (PCs). EDLCs store charges using extremely thin double layer structure composed by the interface between electrodes and electrolytes, while PCs store energy by the reversible redox reactions on the electrode surface [5]. EDLC materials with high electronic conductivity and a large specific surface area have been used to achieve energy storage [6]. Due to the redox reaction, PCs can store more charges. The stored charges of EDLCs on the available surface are 0.17–0.20 electronics/atoms, while those of PCs are about 2.5

electronics/atoms. The stored energy by the PC system theoretically exceeds 10–100 times that of the same mass or volume of carbon-based EDLCs. However, the redox reaction of PCs induces the poor stability and low cycle life.

At present, carbon materials are the mainstream materials for the research and commercial application of EDLCs. They possess a high specific surface area, better electronic conductivity, and high chemical stability and they are abundant, low-cost, easy to process, and nontoxic. Common carbon materials include carbon nanotube (CNT), carbon fiber (CF), template carbon (TC), carbon aerogel (CA) and graphene, and so on [7–11]. Due to only physical adsorption being involved in charge storage, such EDLCs have an excellent charging and discharging stability, and the number of cycles even reaches several hundred thousand. Compared to EDLCs, PCs have a higher Cs and E [12], just for a large number of ions involved in the redox reaction [13]. Conducting polymers are typical PC electrode materials, while metal oxides are both EDLC and PC electrode materials [14–16]. Generally speaking, common conductive polymers include polyaniline, polypyrrole, polythiophene, and so on [17–20]. When charged and discharged, conductive polymers will undergo a rapid redox reaction to achieve the storage, release of charges, and produce a large capacity. The capacitance of conductive polymers is much higher than that of carbon materials. Conductive polymers have the advantages of good conductivity, low cost, abundant sources, and easy processing, but they have an unstable structure and poor cycling stability.

As a kind of PC electrode material, transition metal oxides mainly include RuO_2, Co_3O_4, MnO_2, and Fe_2O_3 [21–24]. As the surface of the atoms will be deposited at the underpotential, the generated charge in this process is just like chemical adsorption. This kind of material undergoes a reversible redox reaction of multiple electrons, so it stores many more charges [25]. Compared to other electrode materials, transition metal oxides have the higher Cs [26]. More and more researchers are studying the electrochemical performance of transition metal oxides. RuO_2 is examined because of its high electrochemical properties [27]. However, its high price limits commercialization, while potential damage to the environment is also a barrier. Thus, other metal oxides have been developed as electrode materials, such as Co_3O_4, MnO_2, Fe_2O_3, and so on [28]. Among them, Co_3O_4 electrode material has been widely studied because of the higher Cs, low price, and environmental friendliness. Furthermore, Co_3O_4 electrode material with special microstructures and morphology possesses an excellent electrochemical capacitive behavior [29]. However, Co_3O_4 electrode material has poor conductivity. In order to overcome the disadvantage of a single electrode material, the preparation of Co_3O_4-containing composites will achieve a superior combination performance [30]. Recently, graphene-based composites have been mostly studied [31] and acted as electrode materials for various energy storage systems [32]. For graphene, 2D porous graphene framework nanomaterials in SCs are a hotspot of recent research [33]. When combined with Co_3O_4 nanomaterial, they show excellent properties in asymmetric SCs [34]. Compared to a single component of Co_3O_4 and graphene, Co_3O_4/graphene composites exhibit a higher specific capacitance, specific energy, and specific power.

In this review, recent progress on Co_3O_4 and Co_3O_4-containing composites is summarized. Firstly, the synthetic methods and electrochemical performance of Co_3O_4 electrode materials are introduced, including the hydrothermal/solvothermal method, sol–gel method, thermal decomposition, chemical precipitation, electrodeposition, chemical bath deposition, and the template method. Then, Co_3O_4-containing electrode materials are summarized, including Co_3O_4/carbon, Co_3O_4/conducting polymer, and Co_3O_4/metal compound composites. The preparation and performance of various composite electrodes are discussed as given in Figure 1. Finally, the current challenges and outlook on Co_3O_4 and Co_3O_4-containing composites are put forward.

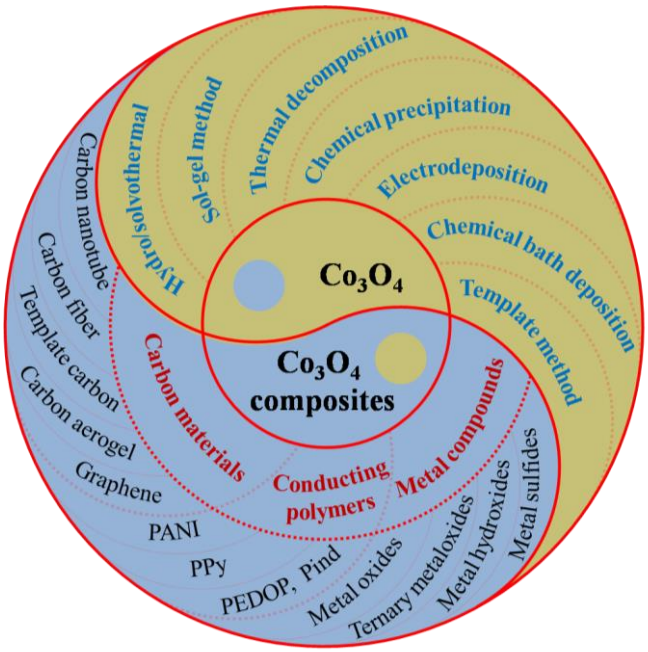

Figure 1. Schematic illustration of Co_3O_4 and Co_3O_4-containing composites materials for supercapacitors (SCs).

2. Synthesis and Performance of Co_3O_4

2.1. Hydrothermal or Solvothermal Method

The hydrothermal method is based on the change of solubility in the sealed heating stainless steel autoclave maintained at a certain temperature and pressure. Reaction temperature, time, pressure, and concentration of reactants will affect the morphology, size, and crystal type of the products [35]. Hydrothermal reaction has been widely used for the synthesis of Co_3O_4 nanomaterials. For example, one-dimensional (1D) nanorod-like Co_3O_4 was successfully synthesized via the hydrothermal method [36]. It had a high Cs of 655 $F{\cdot}g^{-1}$ at a current density of 0.5 $A{\cdot}g^{-1}$ and also exhibited a high capacitance retention and a better cycling stability. Further, two-dimensional (2D) ultrathin mesoporous Co_3O_4 nanosheets were generated on nickel foam (NF) substrate via a hydrothermal technique without any surfactant (Figure 2a) [37]. The Cs of Co_3O_4 nanosheets were as high as 610 $F{\cdot}g^{-1}$ at 1 $A{\cdot}g^{-1}$, and the cycling stability remained at about 94.5% after 3000 cycles at 4 $A{\cdot}g^{-1}$. Moreover, an ultrathin mesoporous Co_3O_4 nanosheet delivered an E of 136 $Wh{\cdot}kg^{-1}$ at the P of 0.75 $kW{\cdot}kg^{-1}$. In addition, a self-assembled microsphere material composed of Co_3O_4 nanosheets was synthesized via the hydrothermal method [38]. It showed a good cycling stability, and the capacitance remained about 101.7% after 1500 cycles at 1.0 $A{\cdot}g^{-1}$. The hydrothermal method was also used to synthesize 2D Co_3O_4 thin sheets consisting of three-dimensional (3D) interconnected nanoflake array [39]. The reaction temperature has a significant impact on the performance of SCs. Under 500 °C for 6 h, 2D Co_3O_4 thin sheets exhibited a Cs of 1500 $F{\cdot}g^{-1}$ at 1 $A{\cdot}g^{-1}$. Capacitance was retained at 99.3% after 2000 cycles at 5 $A{\cdot}g^{-1}$. Furthermore, as an electrode for an asymmetric SC, it exhibited an E of 15.4 $Wh{\cdot}kg^{-1}$ at a P of 0.8 $kW{\cdot}kg^{-1}$.

The difference between the solvothermal and hydrothermal method is that the organic phase is used as a solvent instead of or partially instead of water [40]. Under a high pressure, the physical properties of organic solvents (density, viscosity, and dispersion) will change greatly when compared to the atmospheric pressure condition, thus making it possible for some special chemical reactions to occur. Some solvents often participate in chemical reactions, such as ethanol, isopropanol, etc. At the same time, ethanol can also be used as a reducing agent in the system, and organic solvents can also be combined with reactants to change the state of the reactants. Thus, they affect the morphology, size, and other parameters of product [41]. This method has received extensive attention. For example, a

solvothermal method was adopted to fabricate an ultrafine Co_3O_4 nanoparticle material [42]. These ultrafine Co_3O_4 nanoparticles exhibited a Cs of 523.0 $F{\cdot}g^{-1}$ at 0.5 $A{\cdot}g^{-1}$ and a good cycling stability, and Cs was retained at about 104.9% after 1500 cycles. Recently, Liu et al. [43] successfully fabricated homogeneous core–shell Co_3O_4 mesoporous nanospheres via the solvothermal method (Figure 2b). The core–shell structure effectively promoted electron and ion transmission and alleviated the strain of the Co_3O_4 electrode upon cycling. The Co_3O_4 electrode exhibited a high Cs of 837.7 $F{\cdot}g^{-1}$ at 1 $A{\cdot}g^{-1}$ and a remarkable rate capability. An asymmetric SC was constructed using Co_3O_4 nanowires as a positive and graphene aerogel as a negative electrode, which delivered an E of 35.8 W $h{\cdot}kg^{-1}$ at a P of 797.4 $W{\cdot}kg^{-1}$. Therefore, the solvothermal method provides a novel strategy to prepare Co_3O_4 electrode materials with different nanostructures.

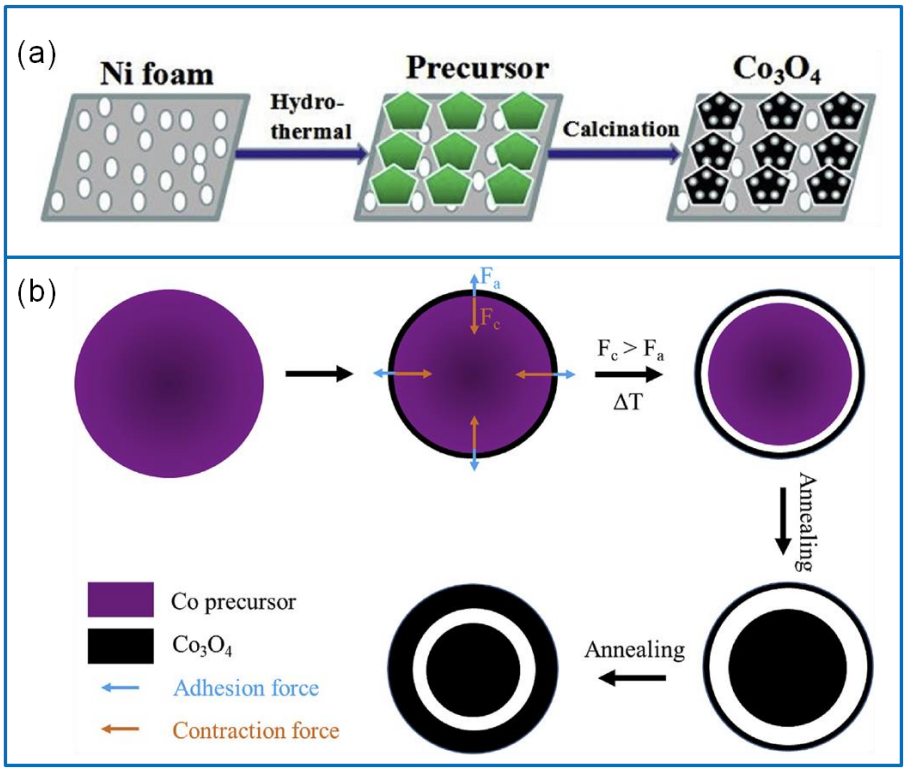

Figure 2. (**a**) Schematic illustration of preparing 2D ultrathin Co_3O_4 nanosheets via the hydrothermal method [37]. (**b**) Schematic illustration of synthesizing core–shell Co_3O_4 mesoporous nanospheres via the solvothermal method [43].

2.2. Sol–Gel Method

The sol–gel method is an important method for the synthesis of Co_3O_4 electrode materials. In a typical sol–gel method, an active precursor is evenly mixed in the liquid phase to form a transparent and stable sol through a hydrolysis and condensation process, and then aging to form a gel [44]. The sol–gel method has some advantages, such as low reaction temperature, ease of operation, miscellaneous and uniform molecular-level mixing, smaller size, and so on [45]. Co_3O_4 nanoparticles with no secondary phase were synthesized via the sol–gel method [46]. The Co_3O_4 nanoparticles delivered a Cs of 120 $F{\cdot}g^{-1}$ at 1 $A{\cdot}g^{-1}$ in a voltage window of 0 to 0.6 V. In addition, Lakehal et al. [47] prepared Co_3O_4 electrode materials by adopting the sol–gel-based dip-coating process on a glass substrate. Meanwhile, the effects of Ni-solution concentrations on the properties of Co_3O_4 samples were studied. The results showed that the resistance of obtained Co_3O_4 polycrystalline decreased in spinel-type, whereas the capacity increased with an increase in Ni doping levels. Peterson et al. [48] prepared Co_3O_4 with different morphologies via the sol–gel method and compared the performance of sphere-like,

sponge-like, network-like, and plate-like Co_3O_4. The network-like sample exhibited a higher Cs of 708 $F{\cdot}g^{-1}$ at 5 $mV{\cdot}s^{-1}$ and a good rate capacity of 71.9% at 50 $mV{\cdot}s^{-1}$.

2.3. Thermal Decomposition

Thermal decomposition is widely used in the synthesis of Co_3O_4 electrode materials. In a typical thermal decomposition method, precursors are prepared by adding inorganic or organic salt solutions, and Co_3O_4 nanoparticles are synthesized via heating the precursors in air or another atmosphere [49]. The precursors gradually decompose into water, carbon dioxide, carbon and monoxide, etc. and leave a large number of Co_3O_4 pore structures. For instance, 1D porous Co_3O_4 nanowires were prepared via the thermal decomposition method with nitrilotriacetic acid (NA) as the chelating agent [50]. The Co_3O_4 nanowires exhibited a high Cs of 2815.7 $F{\cdot}g^{-1}$ at 1 $A{\cdot}g^{-1}$, an ideal rate capacity at 20 $A{\cdot}g^{-1}$, and an excellent coulombic efficiency (about 100%). Further, Ni foam supported Co_3O_4 nanoflakes were prepared via the thermal decomposition method [51]. Firstly, the nanosheet Co particles were deposited on Ni foam. Secondly, dendritic-like CoC_2O_4 nanowires were synthesized via in situ reaction. Finally, the dendritic-like CoC_2O_4 precursors were transformed into Co_3O_4 nanoflakes via the thermal decomposition method. The unique configuration showed a great advantage in terms of porosity and interlocking channels, because it effectively increased the surface contact with the electrolyte and ion/electron diffusion. The Co_3O_4 nanoflakes exhibited a high Cs of 576.8 $F{\cdot}g^{-1}$ at 1 $A{\cdot}g^{-1}$ and about 82% capacitance retention after 5000 cycles.

2.4. Chemical Precipitation

The chemical precipitation method can be classified into three categories: direct precipitation, coprecipitation, and homogeneous precipitation [52]. In a direct precipitation, reactants are directly added into a cobalt salt solution to produce precipitates, and then the product is washed, dried or calcined to obtain Co_3O_4 nanomaterials [53]. The method has the characteristics of simple operation and high product purity. In this regard, Wang et al. [54] prepared 3D-nanonet cobalt carbonate precursors via the direct precipitation method. The precursors were calcined in the air and converted into Co_3O_4 nanoparticles with original frame structures (Figure 3a), which displayed a Cs of 739 $F{\cdot}g^{-1}$ at 1 $A{\cdot}g^{-1}$ and a capacitance retention of 90.2% after 1000 cycles at 5 $A{\cdot}g^{-1}$. The coprecipitation method refers to the deposition of multiple metal ions [55]. Therefore, it is rarely used for the synthesis of a single Co_3O_4 nanomaterial. For the homogeneous precipitation method, metal ions are slowly released to the solution through a chemical reaction. Thus, homogeneous precipitation reactions do not occur immediately between precipitated ions. This overcomes the disadvantage of local inhomogeneity caused by the direct introduction of precipitates. The Co_3O_4 nanomaterials synthesized via homogeneous precipitation have a uniform size distribution and high purity. For example, an ultrathin Co_3O_4 material with high porosity was synthesized via a homogeneous precipitation method [56]. The structure was composed of well-arranged 2D rectangular thin sheets with a high specific surface area, pore volume, and uniform aperture distribution (Figure 3b). The Co_3O_4 thin sheets showed a high Cs of 548 $F{\cdot}g^{-1}$ at 8 $A{\cdot}g^{-1}$, and a capacitance retention of 98.5% after 2000 cycles at 16 $A{\cdot}g^{-1}$. They also exhibited an excellent cyclic stability, structural stability, and electrochemical stability.

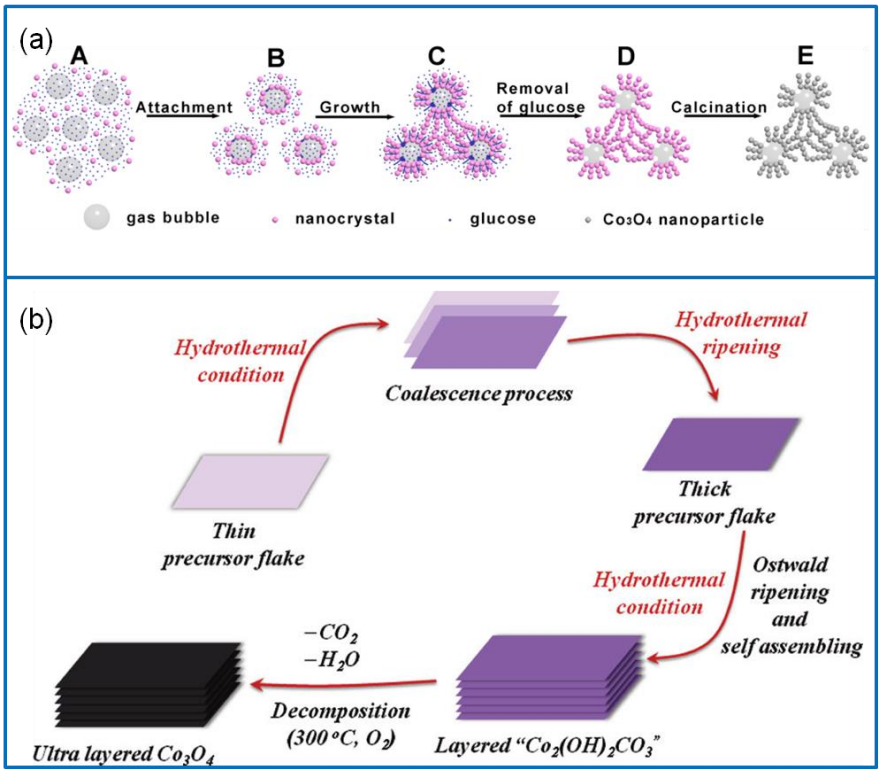

Figure 3. (**a**) Schematic illustration of preparing hollow structure Co_3O_4 via the direct precipitation method [54]. (**b**) Schematic illustration of preparing ultralayered Co_3O_4 via the homogeneous precipitation method [56].

2.5. Electrodeposition

With this method, nanomaterials are deposited on the electrode surface via an electrochemical reduction reaction [57]. The active materials can be evenly distributed on the electrodes through this method. In this technique, the morphology, size, and composition of synthesized nanomaterials are controllable. For example, Co_3O_4 nanoplates were prepared via the electrodeposition method [58]. Initially, $Co(OH)_2$ nanoplates were synthesized through an additive-free electrodeposition route, and then the Co_3O_4 nanoplates were obtained via calcination. The Co_3O_4 nanoplates exhibited a Cs of 485 $F{\cdot}g^{-1}$ and a capacitance retention of 84.1% after 3000 cycles at 5 $A{\cdot}g^{-1}$. Further, a Co_3O_4 nanosheet was prepared through a one-step cathodic electrophoretic deposition of polyethylenimine in aqueous solutions [59]. The electrode showed a Cs of 233.6 $F{\cdot}g^{-1}$ at 0.5 $A{\cdot}g^{-1}$ and a capacitance retention 93.5% after 2000 cycles. Meanwhile, other Co_3O_4 nanosheets were fabricated on Ni foam via the electrodeposition of a $Co(OH)_2$ precursor following annealing [60]. The Co_3O_4 electrode presented a super high Cs of 6469 $F{\cdot}g^{-1}$ at 5 $mA{\cdot}cm^{-2}$, which exceeded its theoretical value. Impressively, it maintained a Cs of 4127 $F{\cdot}g^{-1}$ at 15 $mA{\cdot}cm^{-2}$ and a capacitance retention of 81.6% after 2000 cycles.

2.6. Chemical Bath Deposition

Chemical bath deposition (CBD) is a chemical reduction process. A suitable reducing agent is used to reduce the metal ions in the plating liquid, and the metal ions are deposited on the matrix of the matrix. CBD directly grows quantum dots on substrate, and it is a relatively slow chemical reaction process. Compared to other preparation methods, the CBD method has obvious advantages in its controllability, uniformity, and low cost. Moreover, different substrates and solutions can be used to prepare Co_3O_4 electrode materials [61]. For example, Co_3O_4 nanowire was synthesized on stainless steel (SS) substrate via the CBD method [62], which possessed a high specific surface area of 66.33 $m^2{\cdot}g^{-1}$. It exhibited a high Cs of 850 $F{\cdot}g^{-1}$ at 5 $mV{\cdot}s^{-1}$ and a cycling stability of about 86% after

5000 cycles. The symmetric SC device was fabricated using a Co_3O_4 nanowire, which showed a Cs of 127 $F{\cdot}g^{-1}$, an E of 24.18 $Wh{\cdot}kg^{-1}$, and a cycling stability of 85% after 3000 cycles. In addition, Co_3O_4 nanorod arrays were fabricated via the facile CBD method [63]. The size of the nanorod was about 450 nm. As an electrode, the Co_3O_4 nanorod arrays delivered a Cs of 387.3 $F{\cdot}g^{-1}$ at 1 $A{\cdot}g^{-1}$ and a cyclic stability of 88% after 1000 cycles.

2.7. Template Method

The template method usually adopts a template with a certain morphology and nanostructure. The products are formed on the template, then the template is removed to obtain nanomaterials with the same morphology and size [64]. The most used templates are surfactants, biomolecules, polymers, and a metal–organic framework (MOF) [65]. For example, a 2D hierarchical Co-based MOF of UPC-9 was used to synthesize ultrathin and rich macroporous Co_3O_4 nanosheets [66]. It exhibited a remarkable Cs of 1121 $F{\cdot}g^{-1}$ at 1 $A{\cdot}g^{-1}$ and a rate capability of 77.9% at 25 $A{\cdot}g^{-1}$. This is because the organic ligand of UPC-9 prevents the agglomeration of Co_3O_4 caused by calcination. In addition, another ultrathin Co_3O_4 nanosheet was constructed by the zeolitic imidazolate framework-67 (Figure 4a) [67]. The Co_3O_4 electrode showed a large Cs of 1216.4 $F{\cdot}g^{-1}$ at 1 $A{\cdot}g^{-1}$ and a higher rate capability of 76.1% at 20 $A{\cdot}g^{-1}$. The template method can also be used to prepare other morphological Co_3O_4 electrode materials. The hollow spherical Co-BTB-I and flower-like Co-BTB-II precursors were obtained via the template method with/without hexadecyl trimethyl ammonium bromide (CTAB) (Figure 4b) [68]. After annealing, the Co_3O_4 nanoparticles maintained the template morphologies. The Co-BTB-I electrode exhibited a Cs of 342.1 $F{\cdot}g^{-1}$ at 0.5 $A{\cdot}g^{-1}$. The template method has many advantages; however, it needs more processing steps and has certain requirements on the template.

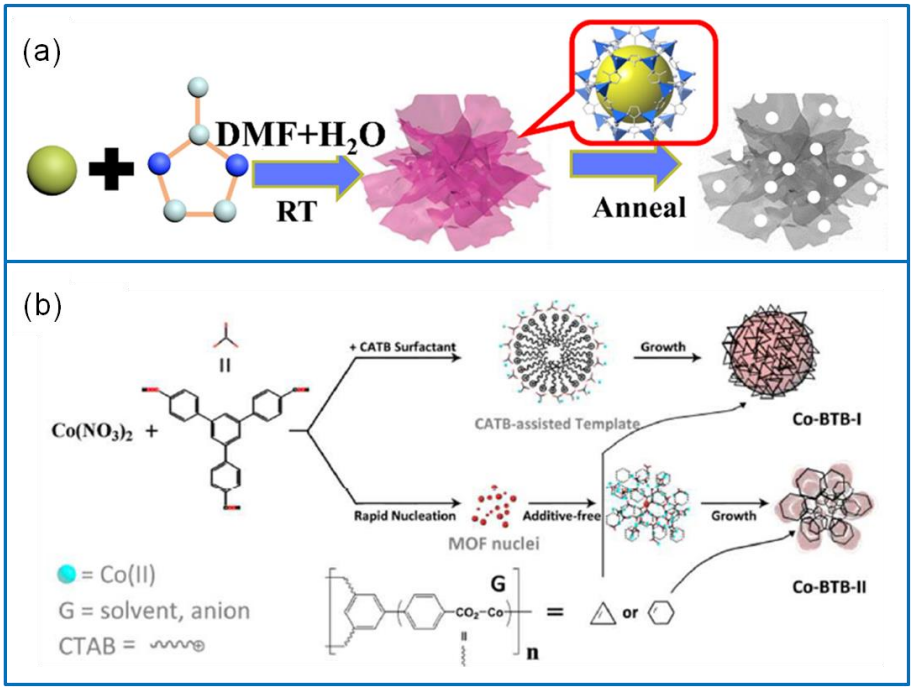

Figure 4. (**a**) Synthesis process of ultrathin Co_3O_4 via the template method [67]. (**b**) Schematic illustration of hollow spherical Co-BTB-I and the flower-like Co-BTB-II [68].

In addition to the above methods, there are other methods to synthesize Co_3O_4, such as spray pyrolysis [69], chemical vapor deposition (CVD) [70], the electrospinning technique [71], galvanic displacement [72], laser ablation [73], the in situ self-organization method [74], and so on. To sum up, there are many synthesis methods for preparing Co_3O_4 electrode materials, which are mainly divided into three categories: the gas phase method, solid phase method, and liquid phase method. The Co_3O_4

electrode materials synthesized via the gas phase method have the advantages of small size, good dispersion, etc. However, they need tough experimental equipment and conditions. The materials prepared via the solid phase method have the advantages of no agglomeration and good filling but have the disadvantages of high energy consumption, low efficiency, and many more impurities. The liquid phase method is one of the most commonly used methods to prepare Co_3O_4 electrode materials. The liquid phase method has the advantages of simple operation, mild conditions, high purity, and good dispersion. However, the development of Co_3O_4 electrode materials is not limited to the laboratory stage; we should consider the industrialization and commercialization of Co_3O_4. The preparation of high-performance Co_3O_4 electrode materials requires tough synthesis conditions, such as, high temperature and pressure, with a small-scale output, which affect the rapid development of industrialization and commercialization to some extent. Therefore, developing a low-cost, rapid, and simple synthesis method is an important task for improving the performance of Co_3O_4.

2.8. Performance Statistics of Different Co_3O_4 Materials

The relationship between the electrochemical performance, synthetic method, and the microstructures of Co_3O_4 is summarized in Table 1. Among them, Co_3O_4 nanoparticles synthesized via the hydrothermal method have a good dispersion, high purity, and high crystallinity. Compared to the hydrothermal method, the solvothermal method tends to synthesize smaller particles. For the sol–gel method, when the gel is formed, the reactants are likely to be evenly mixed at the molecular level, and only low reaction temperature is required. The thermal decomposition method and chemical precipitation method are simple, adaptable, and controllable. The electrodeposition method is generally used to prepare thin film electrodes. Unlike electrochemical deposition, CBD does not require a rectifier power supply and anode. Moreover, the synthesized electrode materials are an almost nanorod structure. As for the template method, as-prepared electrode materials often have a high Cs. Among those Co_3O_4 materials, Co_3O_4 nanosheets prepared via the electrodeposition method displayed an ultrahigh Cs of 6469 $F{\cdot}g^{-1}$ with cycling stability of 81.6% after 2000 cycles [60]. The Co_3O_4 nanospheres synthesized via the solvothermal method exhibited a Cs of 837.7 $F{\cdot}g^{-1}$ at 1 $A{\cdot}g^{-1}$ and an excellent rate capacity of 93.6% at 10 $A{\cdot}g^{-1}$ [43]. Another Co_3O_4 nanosphere showed a cyclic stability greater than 100% after 4000 cycles via the CVD method [70].

Table 1. Electrochemical performance of Co_3O_4 electrode materials.

Synthetic Method	Material Structure	Specific Capacitance	Rate	Cycle Life Retention	Ref.
Hydrothermal	Nanosheet	610 $F{\cdot}g^{-1}$ at 1 $A{\cdot}g^{-1}$	65.7% at 10 $A{\cdot}g^{-1}$	94.5% after 3000 cycles	[37]
Hydrothermal	Nanoflake	1500 $F{\cdot}g^{-1}$ at 1 $A{\cdot}g^{-1}$	55.2% at 10 $A{\cdot}g^{-1}$	99.3% after 2000 cycles	[39]
Solvothermal	Nanoparticle	523.0 $F{\cdot}g^{-1}$ at 0.5 $A{\cdot}g^{-1}$	66.9% at 5 $A{\cdot}g^{-1}$	104.9% after 1500 cycles.	[42]
Solvothermal	Nanosphere	837.7 $F{\cdot}g^{-1}$ at 1 $A{\cdot}g^{-1}$	93.6% at 10 $A{\cdot}g^{-1}$	87.0% after 2000 cycles	[43]
Sol–gel	Nanoparticle	120 $F{\cdot}g^{-1}$ at 1 $A{\cdot}g^{-1}$	_	_	[46]
Sol–gel	Netlike	708 $F{\cdot}g^{-1}$ at 5 $mV{\cdot}s^{-1}$	71.9% at 50 $mV{\cdot}s^{-1}$	_	[48]
Thermal decomposition	Nanowire	2815.7 $F{\cdot}g^{-1}$ at 1 $A{\cdot}g^{-1}$	27.2% at 20 $A{\cdot}g^{-1}$	88.8% after 1100 cycles	[50]
Thermal decomposition	Nanoflake	576.8 $F{\cdot}g^{-1}$ at 1 $A{\cdot}g^{-1}$	49.2% at 50 $A{\cdot}g^{-1}$	82% after 5000 cycles.	[51]
Chemical precipitation	Nanonet	739 $F{\cdot}g^{-1}$ at 1 $A{\cdot}g^{-1}$	72.1% at 15 $A{\cdot}g^{-1}$	90.2% after 1000 cycles	[54]
Chemical precipitation	Ultralayer	548 $F{\cdot}g^{-1}$ at 8 $A{\cdot}g^{-1}$	66% at 32 $A{\cdot}g^{-1}$	98.5% after 2000 cycles	[56]

Table 1. *Cont.*

Synthetic Method	Material Structure	Specific Capacitance	Rate	Cycle Life Retention	Ref.
Electrodeposition	Nanoplate	517 $F{\cdot}g^{-1}$ at 1 $A{\cdot}g^{-1}$	39.1% at 20 $A{\cdot}g^{-1}$	91% after 3000 cycles.	[58]
Electrodeposition	Nanosheet	6469 $F{\cdot}g^{-1}$ at 5 $mA{\cdot}cm^{-2}$	63.8% at 15 $mA{\cdot}cm^{-2}$	81.6% after 2000 cycles	[60]
Chemical bath deposition	Nanowire	850 $F{\cdot}g^{-1}$ at 5 $mV{\cdot}s^{-1}$	~85 at 100 $mV{\cdot}s^{-1}$	86% after 5000 cycles.	[62]
Chemical bath deposition	Nanorod	387.3 $F{\cdot}g^{-1}$ at 1 $A{\cdot}g^{-1}$	33.6% at 5 $A{\cdot}g^{-1}$	88% after 1000 cycles.	[63]
Template	Ultrathin Nanosheet	1121 $F{\cdot}g^{-1}$ at 1 $A{\cdot}g^{-1}$	77.9% at 25 $A{\cdot}g^{-1}$	98.2% after 6000 cycles	[66]
Template	Ultrathin Nanosheet	1216.4 $F{\cdot}g^{-1}$ at 1 $A{\cdot}g^{-1}$	76.1% at 20 $A{\cdot}g^{-1}$	86.4% after 8000 cycles	[67]
Spray pyrolysis	Thin film	412 $F{\cdot}g^{-1}$ at 1 $A{\cdot}g^{-1}$	93% at 4 $A{\cdot}g^{-1}$	92.6% after 1000 cycles	[69]
Chemical vapor deposition	Nanosphere	128 $F{\cdot}g^{-1}$ at 10 $mV{\cdot}s^{-1}$	~90% at 20 $A{\cdot}g^{-1}$	>100% after 4000 cycles	[70]
Electrospinning technique	Nanofiber	340 $F{\cdot}g^{-1}$ at 1 $A{\cdot}g^{-1}$	87.1% at 10 $A{\cdot}g^{-1}$	94% after 1000 cycles	[71]
Galvanic displacement	Ultrathin nanosheet	1095 $F{\cdot}g^{-1}$ at 1 $A{\cdot}g^{-1}$	61.9% at 15 $A{\cdot}g^{-1}$	71% after 2000 cycles	[72]
Laser ablation	Nanosheet	762 $F{\cdot}g^{-1}$ at 6 $A{\cdot}g^{-1}$	82.7% at 36 $A{\cdot}g^{-1}$	-	[73]
In-site self-organization	Nanorods	1486 $F{\cdot}g^{-1}$ at 1 $A{\cdot}g^{-1}$	72.9% at 15 $A{\cdot}g^{-1}$	98.8% after 5000 cycles	[74]

3. Advance of Co_3O_4-Containing Composites

3.1. Co_3O_4/Carbon Composites

3.1.1. Co_3O_4/Carbon Nanotube (CNT) Composites

CNT usually divides into a single-walled carbon nanotube (SWCNT) and multiwalled carbon nanotube (MWCNT). They are seamless hollow tubes that are curled by single-layer or multilayer graphite sheets. They have a unique pore structure, high electrical conductivity, excellent mechanical properties, and prominent surface area utilization and thermal stability, so they are extremely suitable for supercapacitor electrode materials [75]. However, CNT also has some disadvantages, such as a low specific surface area and expensive price. In order to improve its performance, CNT is usually used as carriers to deposit PC materials to prepare composites [76]. Therefore, Co_3O_4/CNT composites have been extensively studied [77]. SWCNT thin film was prepared via a vacuum filtration and continuously stamping method, and then Co_3O_4/SWCNT composite was obtained via the electrodeposition method. It exhibited a Cs of 70.5 $mF{\cdot}cm^{-2}$ at 1 $mV{\cdot}s^{-1}$ and a capacitance retention of 80% after 3000 cycles [78]. Further, Co–Co_3O_4/N–SWCNT core–shell composite was synthesized via simple pyrolysis of cobalt acetate and melamine–formaldehyde resin in N_2 atmosphere [79]. Due to the close contact between the Co–Co_3O_4 nanoparticle cores and the N–SWCNT shells, Co–Co_3O_4@N-SWCNT showed a high Cs of 823.4 $F{\cdot}g^{-1}$ at 1 $A{\cdot}g^{-1}$ and a capacitance retention of 93.6% over 10,000 cycles. Moreover, an asymmetric device of Co–Co_3O_4/ CNT–NC//reduced graphene oxide SC exhibited a high E of 46.7 $Wh{\cdot}kg^{-1}$ at a P of 1601.1 $W{\cdot}kg^{-1}$. In addition, a nitrogen-doped MWCNT/Co_3O_4 composite was prepared in the presence of urea and aqueous ammonia via the thermal decomposition method [80]. The Co_3O_4 nanoparticles were densely dispersed on the N-MWCNT surface. The Co_3O_4/N-MWCNT electrode material exhibited a high Cs of 406 $F{\cdot}g^{-1}$ at 2 $A{\cdot}g^{-1}$ and an excellent capacitance retention of 93% after 10,000 cycles.

3.1.2. Co_3O_4/Carbon Fiber (CF) Composites

CF has a moderately controllable aperture distribution, and its pore structure is suitable for the transfer of electrolyte ions. Thus, it is often used as a carrier of electrode materials [81]. Recently, there has been extensive focus on the development of composite nanofiber materials for enhancing the Cs, E, and P of SCs [82]. For example, a Co_3O_4/CF composite was prepared via the electrospinning method followed by heat treatment [83]. Onion-shaped graphitic layers were formed around the Co_3O_4 nanoparticles, which improved the electrical conductivity of the electrode and prevented the Co_3O_4 nanoparticles from falling from the CF matrix. The Co_3O_4/CF composite delivered a Cs of 586 $F{\cdot}g^{-1}$ at 1 $A{\cdot}g^{-1}$ and a capacitance retention of 74% after 2000 cycles at 2 $A{\cdot}g^{-1}$. Further, 3D Co_3O_4 nanowire arrays were grown on CF via the CVD method (Figure 5a) [84]. The Co_3O_4/CF electrode material exhibited a Cs of 734.25 $F{\cdot}cm^{-3}$ (2210 $mF{\cdot}cm^{-2}$) at 1.0 $A{\cdot}cm^{-3}$. Moreover, all-solid-state fiber-shaped asymmetric SC composed of vanadium nitride nanowires/CF//Co_3O_4/CF exhibited a window of 1.6 V and an E of 13.2 $mWh{\cdot}cm^{-3}$ at 1.0 $A{\cdot}cm^{-3}$. Recently, Co_3O_4/biomass-derived carbon fiber (BCF) with a hierarchical structure was fabricated as shown in Figure 5b [85]. Hollow porous BCF was treated as the sandwich layer, and Co_3O_4 nanoparticles were used for inner and outer cladding. The porous BCF not only provided an ideal electron transfer path to surmount the limit of high resistance of the Co_3O_4 electrode but also served as a backbone, which facilitated the loading of more Co_3O_4 particles to promote the redox reaction. The Co_3O_4/BCF composite delivered a Cs of 892.5 $F{\cdot}g^{-1}$ at 0.5 $A{\cdot}g^{-1}$ and a capacitance retention of 88% over 6000 cycles.

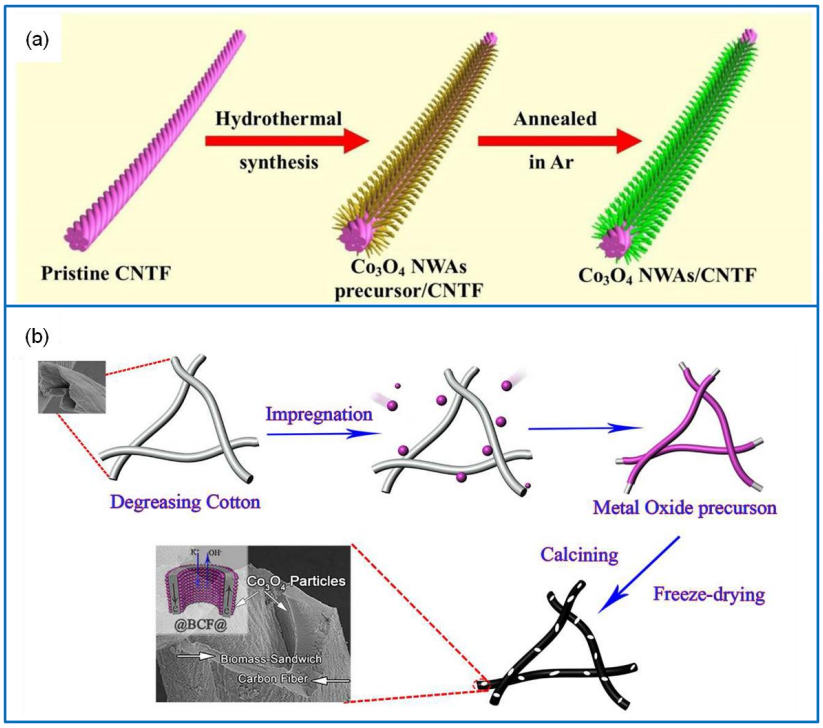

Figure 5. (**a**) Schematic illustration of synthesizing the 3D Co_3O_4 nanowire arrays directly on carbon fibers (CFs) [84]. (**b**) Fabrication of hierarchical Co_3O_4/biomass-derived CF (BCF) electrode material [85].

Carbon cloth (CC) is made of CF. It has the advantages of low cost, good conductivity, light quality, and excellent flexibility [86]. CC can be applied to support cobalt oxide electrode material. The resulting composite can be used directly without secondary processing. This effectively reduces the resistance of the electrode and makes the electrode response good at a high current density. Therefore, CC is widely used in flexible SCs. For example, cobalt oxide was loaded on CC via the cathodic potentiodynamic procedure [87]. The supercapacitor capacity was related to the content of the cobalt

oxide. The composite with 8 wt% cobalt oxide on CC exhibited a Cs of 227 mAh·g^{-1} at 1 mA·cm^{-2} and a capacitance retention of 82% after 5000 cycles.

3.1.3. Co_3O_4/Template Carbon (TC) Composites

At present, TC is commonly used carbon material for SCs [88]. It is a porous carbon material with a uniform and concentrated pore size distribution [89]. There are two ways to prepare TC. The first one is also called active carbon (AC). It is usually derived from physically and chemically activated wood, petroleum coke, phenolic resin, and sucrose. Another is used carbon precursors to infiltrate into template pores, and then the template is removed to obtain porous carbon, which is opposite to the template [90]. Based on the first method, a Co_3O_4/AC composite was synthesized via the microwave-assisted deposition-precipitation method [91]. When the loading of Co_3O_4 is 16.4 wt%, the average size of Co_3O_4 nanoparticles is 7 nm (Figure 6a). This Co_3O_4/AC electrode material presented a Cs of 491 F·g^{-1} at 0.1 A·g^{-1} and a capacitance retention of 89% over 5000 cycles at 5 A·g^{-1} (Figure 6b). Further, a hybrid Co_3O_4/AC electrode material was synthesized from alginate and cobalt salt via a simple self-crosslinking and pyrolysis method (Figure 6c) [92]. The Co_3O_4/AC hybrid material prepared by alginate had the advantages of low cost, a simple manufacturing process, and excellent electrochemical performance. In addition, 3D carbon foam is excellent AC material, and it is prepared via the carbonization of phenolic foam [93]. The unique structure increases the stored amount of charges. For example, a cobalt oxide/carbon foam composite was prepared using the solvothermal method [94], which had a wide pore size distribution and a large specific surface area. It exhibited a high Cs of 115 mAh·g^{-1} at 0.5 A·g^{-1}, a rate capability of 73 mAh·g^{-1} at 10 A·g^{-1}, and a capacitance retention of 86% at 1 A·g^{-1} after 6000 cycles.

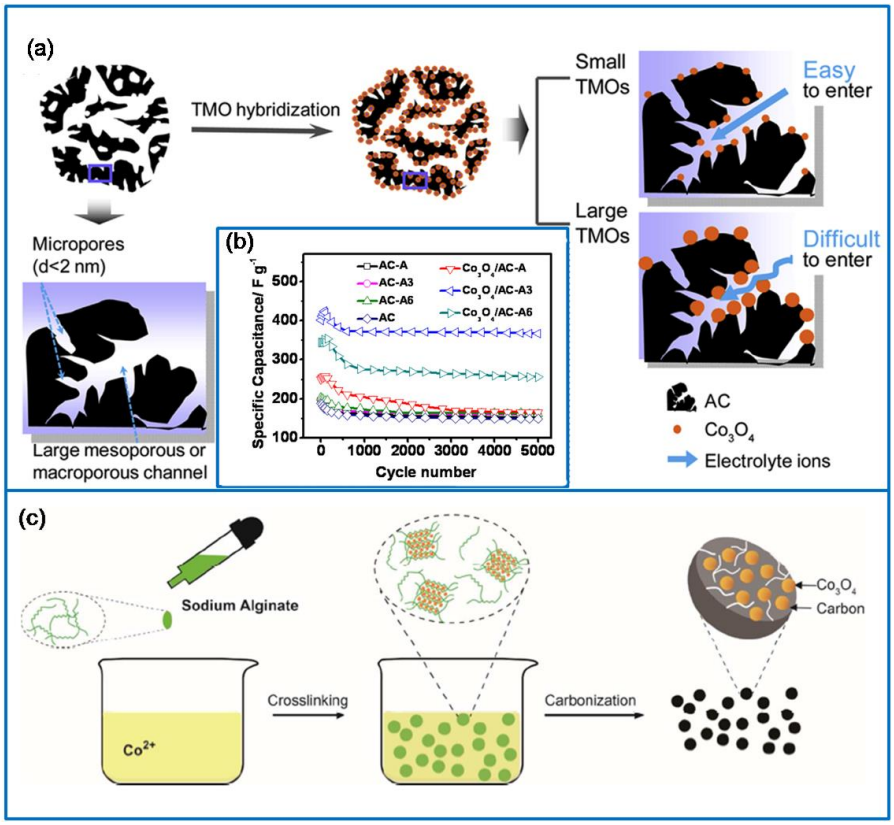

Figure 6. (**a**) Schematic of controlling the Co_3O_4 particles size. (**b**) The cycling life performance of AC- and Co_3O_4/AC-based electrodes at 5 A·g^{-1} [91]. (**c**) Synthesis process of the Co_3O_4/AC electrode materials [92].

Using the carbon precursors, a 3D hierarchical carbon skeleton/Co_3O_4 composite was prepared [95]. The 3D hierarchical carbon skeleton was fabricated on the silica nanosphere templates via thermal vapor deposition. Phosphoric acid was employed to control its porosity and surface area. The TC electrode exhibited a Cs of 134 $F{\cdot}g^{-1}$ at 10 $mV{\cdot}s^{-1}$, while the resulting composite had an enhanced Cs of 456 $F{\cdot}g^{-1}$ at 1 $A{\cdot}g^{-1}$. Further, a zeolitic imidazolate framework-67 precursor was used to synthesize the Co_3O_4/TC composite, which exhibited a high Cs of 885 $F{\cdot}g^{-1}$ at 2.5 $A{\cdot}g^{-1}$ and a capacitance retention of 94% over 10,000 cycles [96]. Recently, a mesoporous carbon (CMK-3) was prepared via the hard template of silica SBA-15, and the silica template was removed via HF [97]. The Co_3O_4/CMK-3 composite was grown on NF by a hydrothermal and annealing process. It exhibited a high Cs of 1131.3 $F{\cdot}g^{-1}$ at 0.5 $A{\cdot}g^{-1}$ and a capacitance retention of 91% after 3000 cycles, while the bare Co_3O_4 film delivered a Cs of 727 $F{\cdot}g^{-1}$ and 82% capacitance retention.

3.1.4. Co_3O_4/Carbon Aerogel (CA) Composites

CA is a kind of nanoporous amorphous material; it has a unique three-dimensional network structure, with light weight, a large specific surface area, good conductivity, and rich dielectric electrochemical stability [98]. For hierarchical porous CA, macropores can promote electron transmission to increase the specific power, while mesopores and micropores are responsible for providing large specific surface areas to increase the E. In the field of Co_3O_4/CA composites, a hybrid Co_3O_4/CA electrode was synthesized via the in situ growth method [99]. The Co_3O_4/CA electrode material exhibited a Cs of 350 $F{\cdot}g^{-1}$ at 1 $A{\cdot}g^{-1}$ and an E of 23.82 $kW{\cdot}kg^{-1}$ at a P of 95.96 $W{\cdot}kg^{-1}$. In a symmetrical SC device, it could be cycled reversibly in a voltage window of 0.0 to 1 V at 1 $A{\cdot}g^{-1}$ and exhibit a capacity retention of 210% over 6000 cycles. Furthermore, CA can be modified by other materials. For example, a novel high-performance Co_3O_4/nitrogen-doped carbon aerogel (NCA) electrode material was prepared via the in situ coating method followed by the freeze-drying process [100]. The Co_3O_4/NCA composite exhibited a Cs of 616 $F{\cdot}g^{-1}$ at 1 $A{\cdot}g^{-1}$ and an excellent rate capability of 445 $F{\cdot}g^{-1}$ at 20 $A{\cdot}g^{-1}$. The assembled asymmetric Co_3O_4/NCA//NCA SC device could be cycled in a range of 1.5 V with an E of 33.43 $Wh{\cdot}kg^{-1}$ at a P of 375 $W{\cdot}kg^{-1}$. Further, a hierarchical porous carbonaceous aerogel (HPCA) was fabricated using renewable seaweed aerogel [101]. It possessed a hierarchical micro/meso/macroporous structure and a high specific surface area of 2200 $m^2{\cdot}g^{-1}$. The HPCA exhibited a Cs of 260.6 $F{\cdot}g^{-1}$ at 1 $A{\cdot}g^{-1}$ and a capacitance retention of 91.7% over 10,000 cycles at 10 $A{\cdot}g^{-1}$. When the HPCA was used to grow Co_3O_4 nanowires, the Co_3O_4/HPCA exhibited a high Cs of 1167.6 $F{\cdot}g^{-1}$ at 1 $A{\cdot}g^{-1}$.

3.1.5. Co_3O_4/Graphene Composites

Graphene has a high specific surface area and excellent mechanical properties and electrochemical properties. It shows excellent properties and has great potential in the application of SC [102]. Compared with other materials, graphene has a high conductivity, high carrier mobility, and excellent mechanical strength. Graphene and its derivatives can be directly used as electrode materials for SCs [103]. However, graphene undergoes irreversible agglomeration and restacking during the combination. Discovering how to avoid the agglomeration and stacking problem of graphene is the key to preparing high-performance graphene electrodes [104]. The combination of graphene with metal oxides is an effective way to solve these problems [105]. For example, a hybrid Co_3O_4 nanosheet on the graphene@NF electrode was designed via the in situ synthesis method (Figure 7a) [106]. Due to the different surface diffusion coefficients of Co_3O_4 nanoparticles, the thickness of Co_3O_4 nanosheets can be reduced from 70 to 13 nm with an increase of graphene sheets. The Co_3O_4/graphene@Ni hybrid composite with a 13 nm thick nanosheet exhibited a high Cs of 1.75 $F{\cdot}cm^{-2}$ at 1 $mA{\cdot}cm^{-2}$ and a capacitance increase of 12.2% after 5000 cycles at 10 $mA{\cdot}cm^{-2}$. As a typical carbon material, reduced graphene oxide (rGO) has a high dielectric constant and chemical stability. It has been used as an encapsulator to improve the electrochemical properties of SCs. A Co_3O_4/rGO electrode composite was fabricated via the temperate coprecipitation method. GO was used as a substrate, and a ZIF-67

rhombic dodecahedron was used as the template (Figure 7b) [107]. The Co_3O_4/rGO composite electrode exhibited a Cs of 546 $F \cdot g^{-1}$ at 0.5 $A \cdot g^{-1}$, a rate capability of 90.8% at 5 $A \cdot g^{-1}$, and a capacitance retention of 90% over 10,000 cycles at 5 $A \cdot g^{-1}$.

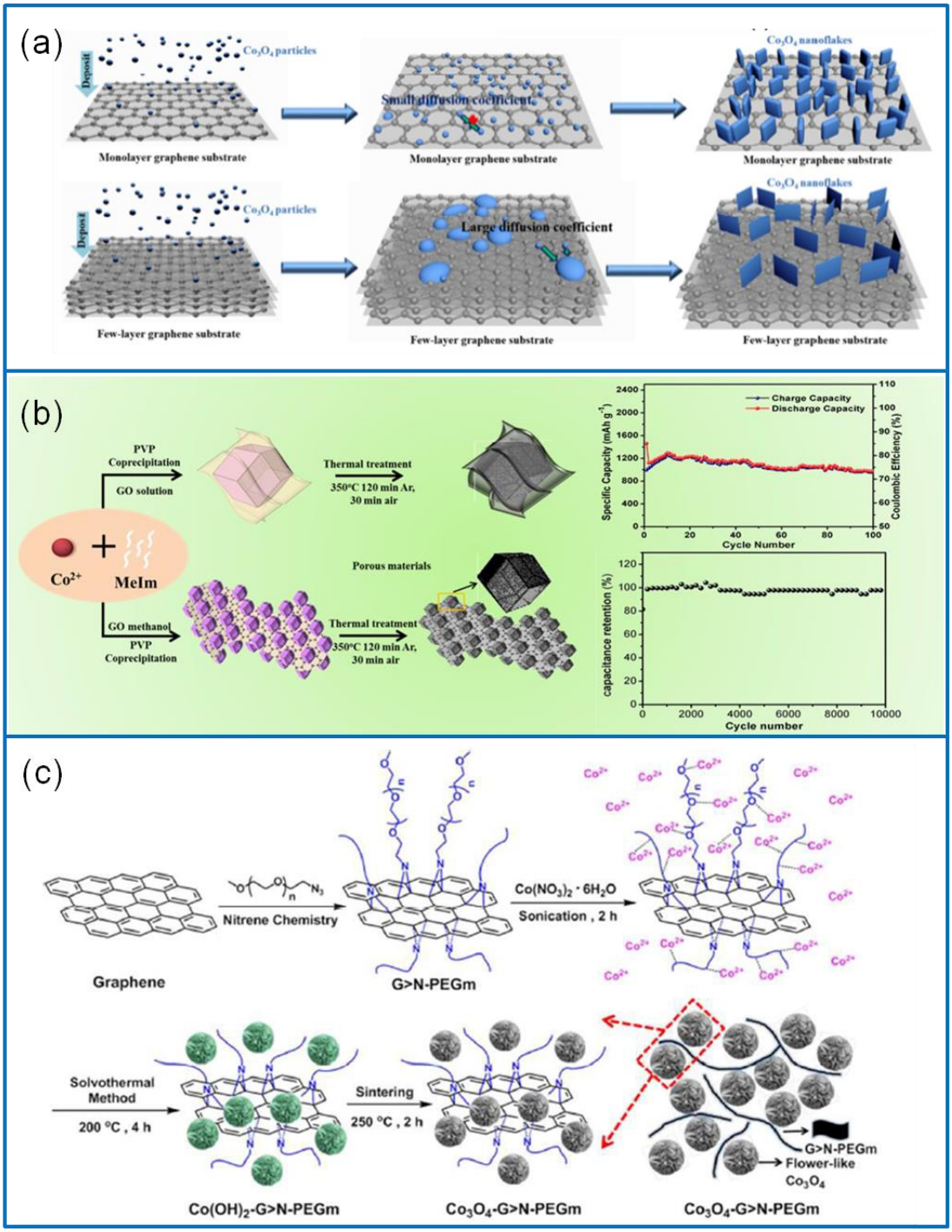

Figure 7. (**a**) Schematic illustration of synthesizing Co_3O_4/graphene@Ni electrode materials via the in situ synthesis method [106]. (**b**) Schematic route to prepare the Co_3O_4/rGO electrode composites [107]. (**c**) Modifying process of Co_3O_4-G > N electrode material by mPEG [108].

Improving E under high P is an urgent problem in the design of SCs. Graphene and its derivatives have done well in this field. A Co_3O_4/graphene composite was hydrothermally deposited on an NF substrate [34]. The cross-linked porous Co_3O_4 nanofiber array on the graphene sheet showed a good boost of performance. The pseudocapacitive Co_3O_4/graphene electrode offered a high Cs of 1935 $F{\cdot}g^{-1}$ at 5 $A{\cdot}g^{-1}$, a rate capability retention of 68% within 0.5–50 $A{\cdot}g^{-1}$, and a capacitance decline of 17% within 2000 cycles. The assembled asymmetric Co_3O_4/grapheme//AC device exhibited an E of 50.3 $Wh{\cdot}kg^{-1}$ at a P of 786 $W{\cdot}kg^{-1}$. Additionally, a Co_3O_4/nitrogen-doped graphene (G > N) composite was synthesized via the solvothermal method [108]. The flower-like Co_3O_4 was loaded on the G > N nanosheets, which were modified with methoxypolyethylene glycol (mPEG) (Figure 7c). The Co_3O_4/G > N electrode materials exhibited a high Cs of 1625.6 $F{\cdot}g^{-1}$ at 0.5 $A{\cdot}g^{-1}$. Particularly, the assembled asymmetric Co_3O_4-G > N//rGO-CNT > N aerogel device exhibited an E of 34.4 $Wh{\cdot}kg^{-1}$ at a P of 400 $kW{\cdot}kg^{-1}$.

3.2. Co_3O_4/Conductive Polymer Composites

Conductive polymers mainly include polyaniline (PANI), polypyrrole (PPy), polythiophene (PTh), and their derivatives. They have advantages of high stability, ease of process, and excellent electrochemical properties. Thus, they are often used as electrode materials [109]. However, conductive polymers lose their conductivity due to electrode damage caused by the embedding and deactivation of anti-ions during circular charging and discharging. This reaction characteristic limits the development of conductive polymers in SCs. In order to further improve the electrochemical performance of conductive polymers, researchers have generally attempted to prepare Co_3O_4/conducting polymer composites [110].

3.2.1. Co_3O_4/PANI Composites

PANI has a good conductivity, high specific capacitance, and high oxidation activity [111]. It is the most widely used conductive polymer in combination with Co_3O_4 composites [112]. A core–shell structured Co_3O_4/PANI electrode material with excellent electrical conductivity and ion diffusion behavior was synthesized via the in situ polymerization method (Figure 8a) [113]. It exhibited a high Cs of 1184 $F{\cdot}g^{-1}$ at 1.25 $A{\cdot}g^{-1}$ and a capacitance retention of 84.9% after 1000 cycles. Furthermore, a hierarchical hollow Co_3O_4/PANI electrode material was also prepared via the in situ polymerization route (Figure 8b) [114]. Due to the excellent conductivity of PANI and hollow nanocage structure, the electron transport rate and specific surface area of the Co_3O_4/PANI electrode material were improved. The contact resistance and charge-transfer resistance of Co_3O_4/PANI electrode material were significantly lower than those of the pristine Co_3O_4. The Co_3O_4/PANI electrode material exhibited a high Cs of 1301 $F{\cdot}g^{-1}$ at 1 $A{\cdot}g^{-1}$ and a cycling retention of 90% after 2000 cycles. The assembled Co_3O_4/PANI//AC device delivered an E of 41.5 $Wh{\cdot}kg^{-1}$ at 0.8 $kW{\cdot}kg^{-1}$, and a P of 15.9 $kW{\cdot}kg^{-1}$ at 18.4 $Wh{\cdot}kg^{-1}$. In addition, a Co_3O_4/PANI layered thin film was successfully prepared on SS substrate via the electrodeposition technique in 0.5 M Na_2SO_4 electrolyte [115]. Compared to the original Co_3O_4 electrode material, it exhibited nearly a 50% increase in the Cs and a significant enhancement of E and P. Particularly, the layered composite electrode showed a capacitance retention of 100% after 500 cycles.

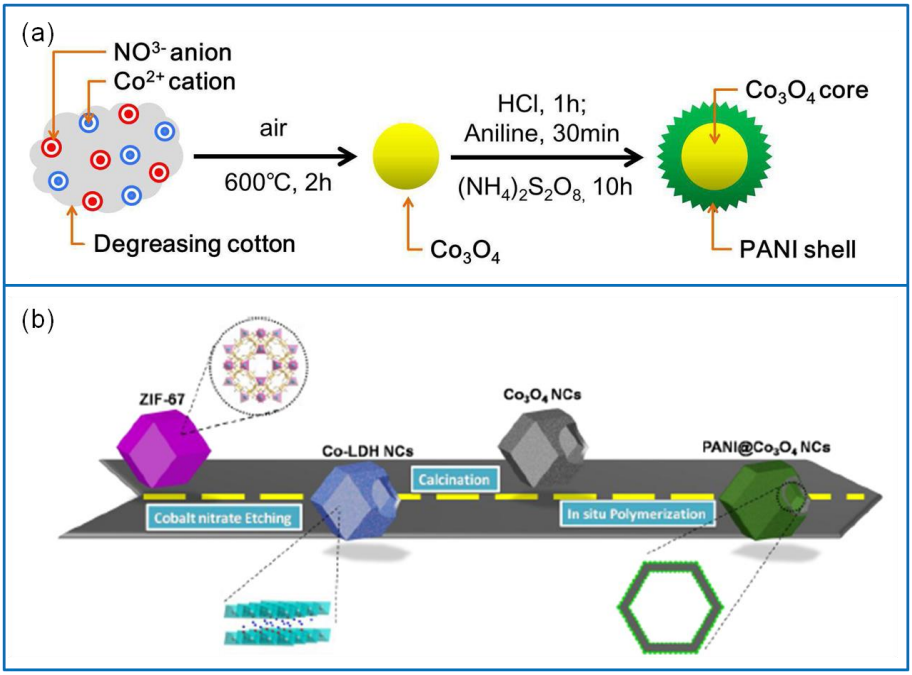

Figure 8. (**a**) Preparation of core–shell structured Co_3O_4/ polyaniline (PANI) electrode material via the in situ polymerization method [113]. (**b**) Schematic illustration of synthesizing hierarchically hollow Co_3O_4/PANI electrode material via the in situ polymerization route [114].

3.2.2. Co_3O_4/PPy Composites

PPy is a new conductive polymer; it has the advantages of good environmental stability, high conductivity, easy synthesis, good extensibility, and excellent electrical characteristic [116]. A lot of works have been reported on Co_3O_4/PPy composites [117]. A hierarchical Co_3O_4/PPy nanowire composite was successfully prepared via in situ chemical polymerization with a template-free hydrothermal route [118]. The Co_3O_4 nanowires were evenly generated on an ultrathin layer of amorphous PPy (Figure 9a). The Co_3O_4/PPy composite had highly electronic conductivity and electroactivity, which could significantly increase active sites and reduce charge transfer resistance. On the basis of these merits, the Co_3O_4/PPy electrode material exhibited a high Cs of 2122 $F{\cdot}g^{-1}$ at 5 $mA{\cdot}cm^{-2}$ and a capacitance retention of 77.8% after 5000 cycles at 25 $mA{\cdot}cm^{-2}$. In addition, a unique Co_3O_4/PPy core–shell nanorod electrode material was prepared via the hydrothermal and electrochemical deposition method [119]. The SC device was fabricated using Co_3O_4/PPy as the positive electrode and active CF as the negative electrode. Due to a wide voltage window of 1.5 V, the device exhibited a high areal capacitance of 1.02 $F{\cdot}cm^{-2}$ and a perfect cycling stability of 98% after 5000 cycles at 50 $mA{\cdot}cm^{-2}$. Recently, a flexible, high-performance, and tailored nanorod solid-state SC was assembled using a Co_3O_4/PPy electrode, a porous carbon electrode, and the PVA electrolyte (Figure 9b) [120]. Benefiting from the Co_3O_4 nanorods and conductive PPy layer, the Co_3O_4/PPy electrode material exhibited a high areal capacitance of 6.67 $F{\cdot}cm^{-2}$ at 2 $mA{\cdot}cm^{-2}$. Moreover, the solid-state SC can be tailored into multiple units and various shapes.

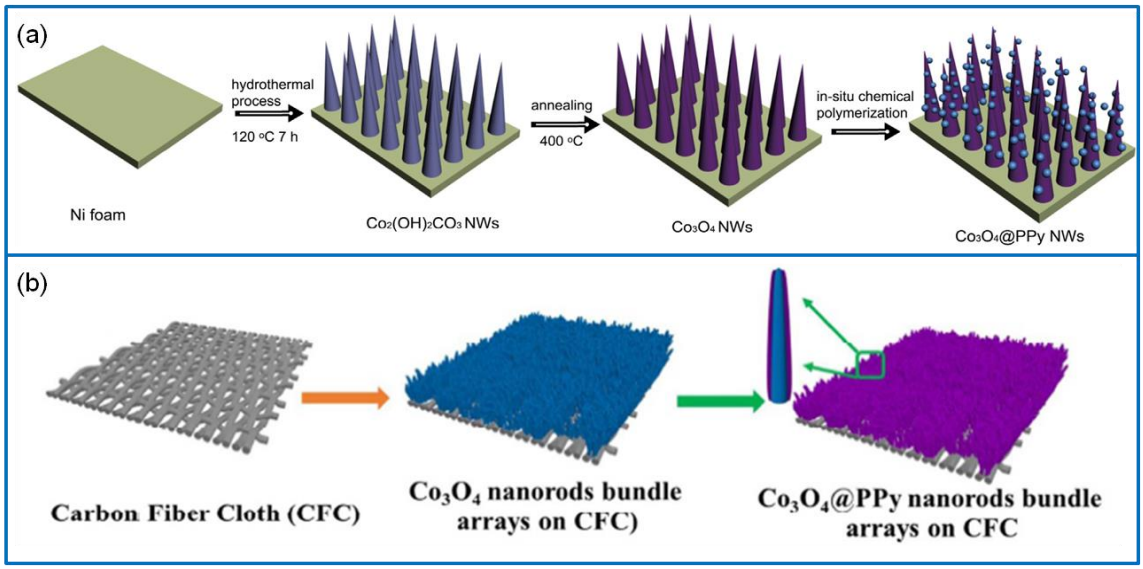

Figure 9. (**a**) Schematic illustration of preparing the hierarchical Co_3O_4/polypyrrole (PPy) core–shell composite nanowires [118]. (**b**) Fabrication of a flexible, high-performance, and tailorable nanorod Co_3O_4/PPy electrode [120].

3.2.3. Co_3O_4/Other Conductive Polymer Composites

The poly(3,4-ethylenedioxythiophene) (PEDOT) has attracted wide attention in recent years. It has a high conductivity, rapid redox, good stability, good film formation, and a high specific surface area. The Co_3O_4/PTh composite was synthesized via in situ chemical oxidative polymerization [121]. In addition, the Co_3O_4/PEDOP nanorod was fabricated on flexible carbon–fabric substrates [122], which delivered a Cs of 407 $F{\cdot}g^{-1}$ at 1 $A{\cdot}g^{-1}$, a retention of 78% over 5000 cycles, and an E of 29.9 $Wh{\cdot}kg^{-1}$ at a P of 0.15 $kW{\cdot}kg^{-1}$. Further, polyindole (Pind) is a common conductive polymer material. A Co_3O_4/Pind electrode material was prepared via the in situ cathodic electrodeposition method [123]. The Co_3O_4/Pind exhibited a high Cs of 1805 $F{\cdot}g^{-1}$ at 2 $A{\cdot}g^{-1}$ and an excellent rate capability of 1625 $F{\cdot}g^{-1}$ at 25 $A{\cdot}g^{-1}$.

3.3. Co_3O_4/Metal Compound Composites

3.3.1. Co_3O_4/Metal Oxide Composites

Metal oxide electrode materials are considered to hybridize with Co_3O_4 [124]. Thus, more and more metal oxides composites containing Co_3O_4 have been reported, such as RuO_2, NiO, Fe_2O_3, ZnO, CuO, MnO_2, SnO_2, and CoO [125–130]. For example, a fish thorn-like nonstructural Co_3O_4/NiO electrode material was successfully synthesized [131] with a core–shell-like structure of NiO nanosheet arrays (NiO/Co_3O_4/NiO) (Figure 10a). It exhibited a Cs of 313.9 $\mu Ah{\cdot}cm^{-2}$ at 4 $mA{\cdot}cm^{-2}$. The assembled NiO/Co_3O_4/NiO//AC device showed a Cs of 623.5 $mF{\cdot}cm^{-2}$ at 2 $mA{\cdot}cm^{-2}$, an E of 216.1 $\mu Wh{\cdot}cm^{-2}$ at a P of 27.7 $mW{\cdot}cm^{-2}$, and a prominent capacity retention of 126% over 5000 cycles. Furthermore, a hierarchical flower-like Co_3O_4/ZnO nanobundle electrode was synthesized via the hydrothermal method [132] (Figure 10b). It exhibited a remarkable Cs of 1983 $F{\cdot}g^{-1}$ at 2 $A{\cdot}g^{-1}$ and a capacitance retention of 84.5% at 10 $A{\cdot}g^{-1}$ over 5000 cycles. The Co_3O_4/ZnO//graphene asymmetric Sc device showed an ultrahigh E of 70.4 $Wh{\cdot}kg^{-1}$ at a P of 779.8 $W{\cdot}kg^{-1}$.

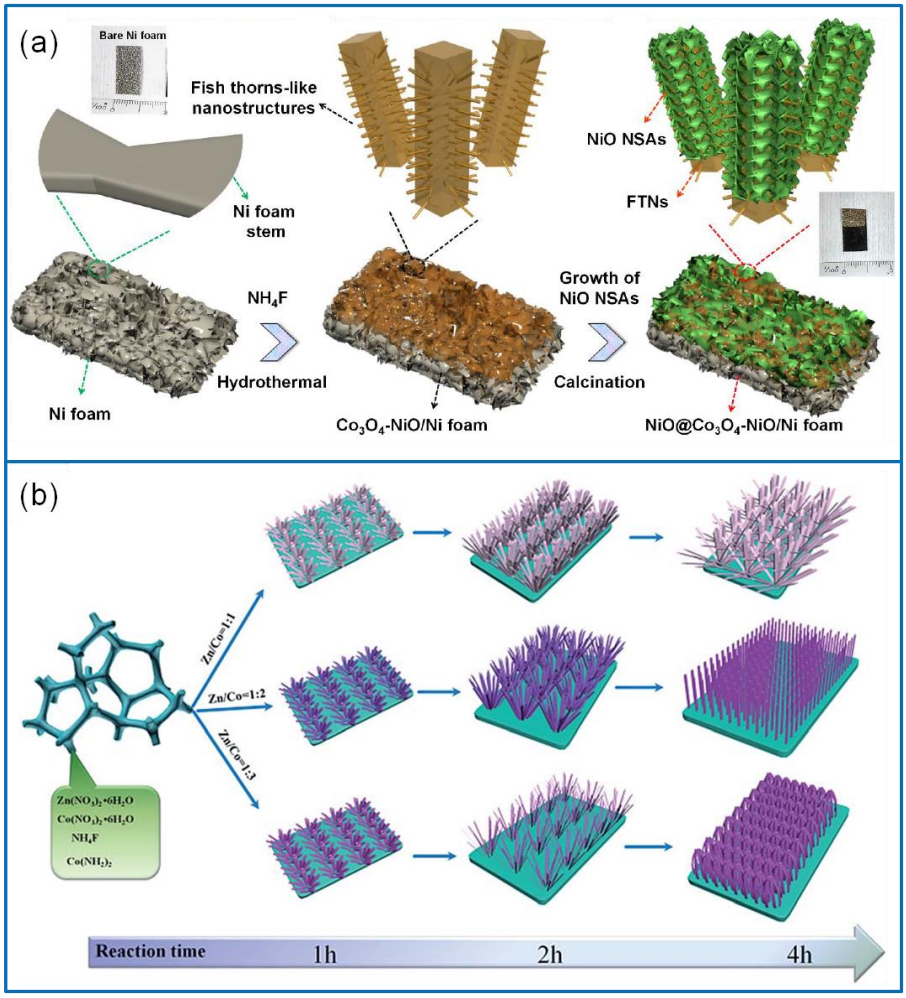

Figure 10. (**a**) Schematic illustration of forming NiO/Co_3O_4/NiO core–shell-like electrode material [131]. (**b**) Schematic route to synthesize hierarchical flower-like Co_3O_4/ZnO nanobundles [132].

Further, a Co_3O_4/CuO electrode with a 1D nanowire morphology was prepared via the electrospinning technique [133]. The Cs values were 712, 1104, and 1242 F·g^{-1} for CuO, Co_3O_4, and Co_3O_4/CuO electrode materials at 2 mV·s^{-1}, respectively. Moreover, the Co_3O_4/CuO//AC device exhibited a high E of 44 Wh·kg^{-1} at a P of 14 kW·kg^{-1} and a capacitive retention of 99% after 2000 cycles at 5 A·g^{-1}. These were related to the voltage window of 1.6 V. For Co_3O_4/CoO electrode material, a Co_3O_4/CoO core–shell nanocrystal with a unique mesoporous microsphere structure was prepared via the solvothermal method following annealing treatment [134]. It exhibited an ultrahigh Cs of 3377.8 F·g^{-1} at 2 A·g^{-1}. Furthermore, the Co_3O_4/CoO//graphene device delivered a high E of 44.06 Wh·kg^{-1} at a P of 800 W·kg^{-1}. As for MnO_2, the Co_3O_4/MnO_2 core–shell arrays were grown on NF for SC via the two-step hydrothermal method [135]. It showed a high Cs of 1920 F·g^{-1} at 1 A·g^{-1} and a capacitance retention of 95.2% after 3000 cycles.

In addition to the composites of metal oxide and Co_3O_4, doped Co_3O_4 has been reported. Metal doping is that the metal ions enter the interior of the Co_3O_4 crystal and substitute Co atom without changing the crystal structure [136]. Metal doping mainly involves Mn [137], Fe [138], and Cd [139]. An Mn-doped Co_3O_4 mesoporous nanoneedle was prepared via the one-step hydrothermal method followed by annealing the precursor on NF [140]. The Mn-doping Co_3O_4 electrode material showed an excellent retention of 104% after 10,000 cycles at 6 A·g^{-1}. Further, Fe-doping Co_3O_4 electrode material was hydrothermally synthesized [138], which exhibited a high Cs 1997 F·g^{-1} at 1 A·g^{-1} and an excellent rate capability of 1757 F·g^{-1} at 20 A·g^{-1}. When tested in the voltage window of 0–1.8 V,

the SC device delivered an E of 270.3 Wh·kg^{-1} at 224.2 Wh·kg^{-1} and a retention of 91.8% over 10,000 cycles at 10 A·g^{-1}.

3.3.2. Co_3O_4/Ternary Metal Oxide Composites

Compared to common metal oxide, ternary metal oxide has a better conductivity and higher redox activity in water electrolytes [141]. These mainly include $NiCo_2O_4$ $NiMoO_4$, $CoWO_4$, $ZnCo_2O_4$, $ZnFe_2O_4$, $CoFe_2O_4$, $CoMn_2O_4$ $MnCo_2O_4$, etc. [142–144]. These ternary metal oxides are often used as SCs electrode materials combining with Co_3O_4 [145–149]. For example, a hierarchical core–shell $Co_3O_4/NiCo_2O_4$ electrode material was successfully fabricated on NF [150]. It exhibited an excellent Cs of 1330 F·g^{-1} at 3 mA·cm^{-2} and a capacity retention of about 100.7% over 5000 cycles. Further, tube-like yolk–shell $Co_3O_4/NiMoO_4$ electrode material was synthesized via the two-step method [151], which consisted of ultrathin porous shell of $NiMoO_4$ and Co_3O_4 fiber (Figure 11a). Benefitting from the unique structure and the synergistic effect of $NiMoO_4$ nanosheets and Co_3O_4 fibers, the $Co_3O_4/NiMoO_4$ electrode exhibited a Cs of 913.25 F·g^{-1} at 10 A·g^{-1}, a capacitance retention of 88% at the current density ranging from 0.5 to 20 A·g^{-1}, and a cycling stability of 89.9% over 3000 cycles at 20 A·g^{-1}. As for $CoWO_4$, 3D $CoWO_4/Co_3O_4$ heterostructure electrode material was synthesized via the microwave hydrothermal method [152] (Figure 11b). It showed a high capacitance of 4.665 F·cm^{-2} at 2.7 mA·cm^{-2} and a rate performance of 70.83% at 27 mA·cm^{-2}. Moreover, the device was composed of the porous carbon as anode and $CoWO_4/Co_3O_4$ as cathode, which exhibited a high E of 45.6 Wh·kg^{-1} at a P of 750 W·kg^{-1}, and a capacitance retention of 90.5% after 5000 cycles.

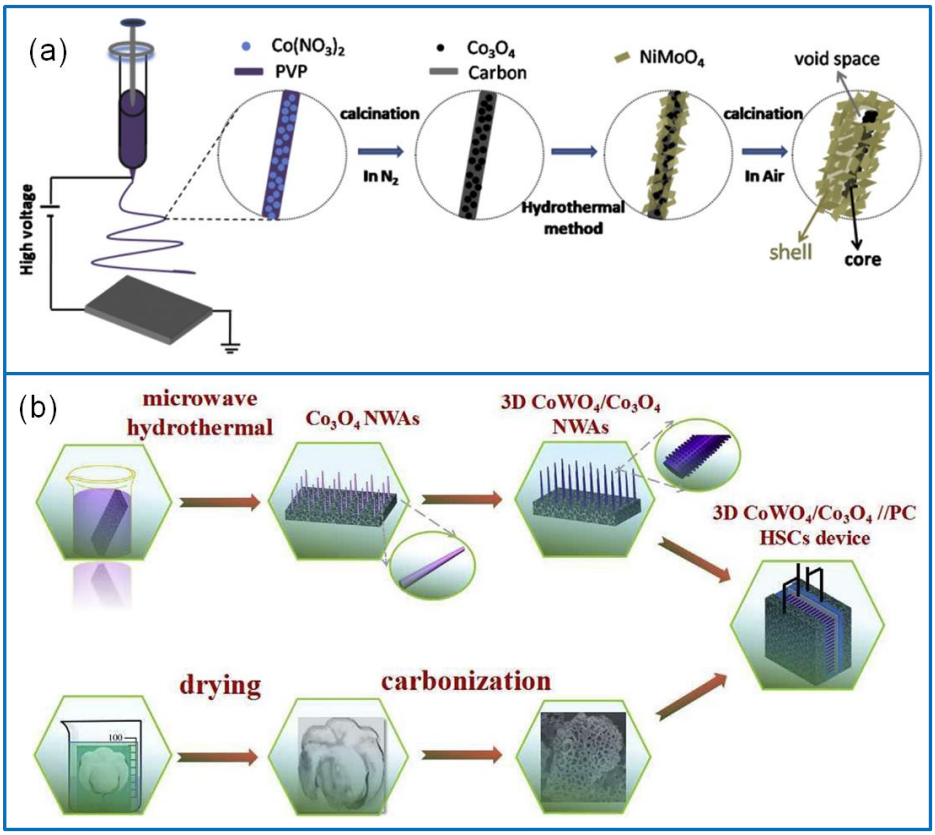

Figure 11. (**a**) Schematic illustration of preparing the $Co_3O_4/NiMoO_4$ electrode materials [151]. (**b**) Fabrication of 3D heterostructure $CoWO_4/Co_3O_4$//porous carbon SC device via the microwave hydrothermal method [152].

In addition, a hollow starfish-shaped porous $Co_3O_4/ZnFe_2O_4$ electrode material was reported [153]. It exhibited a Cs of 326.7 F·g^{-1} at 1 A·g^{-1}, a capacitance retention of 51.8% at 10 A·g^{-1}, a cycling

capacitance retention of 80.7% after 1000 cycles, and a high E of 82.5 Wh·kg^{-1} at a P of 675 W·kg^{-1}. The performance of the $Co_3O_4/ZnFe_2O_4$ composite was much higher than that of the single component. Recently, Sapna et al. [154] synthesized a heterostructured $Co_3O_4/CoFe_2O_4$ electrode material using the hydrothermal method. It exhibited a high Cs of 761.1 F·g^{-1} at 10 mV·s^{-1} and a capacitance retention of 92.2% after 1000 cycles. In another work, a 3D hierarchical shell/core nanosheet/nanoneedle $Co_3O_4/CoMn_2O_4$ electrode material was synthesized on NF [155]. It exhibited a high Cs of 1627 F·g^{-1} at 1 A·g^{-1}, a rate capability of 84.6% at 10 A·g^{-1}, and a capacitance retention of 87.6% over 3000 cycles at 4 A·g^{-1}. The assembled asymmetric $Co_3O_4/CoMn_2O_4$//AC SC device showed a Cs of 125.8 F·g^{-1} at 1 A·g^{-1}, a retention of 89.2% after 5000 cycles at 2 A·g^{-1}, and a high E of 44.8 W h·kg^{-1} at a P of 800.5 W·kg^{-1}. In particular, the $MnCo_2O_4/Co_3O_4$ nanoneedle was synthesized via the template method following thermal annealing in air [156]. It exhibited a high Cs of 1440 C·cm^{-2} at 1 mA·cm^{-2} and a capacitance retention of 82.76% after 8000 cycles. Furthermore, the assembled $Co_3O_4/MnCo_2O_4$//AC SC device exhibited a high E of 31 Wh kg^{-1} at a P of 208.5 W·kg^{-1}, and a capacitance retention of 101.23% after 8000 cycles.

3.3.3. Co_3O_4/Metal Hydroxide Composites

Metal hydroxide mainly relies on a highly reversible redox reaction on the surface and in the body phase to store energy [157]. It is abundant and environmentally friendly and has an important application value in SCs [158]. For example, 3D nonstructural $Co_3O_4/Co(OH)_2$ electrode material was synthesized using the hydrothermal method following electrodeposition (Figure 12a) [159]. It exhibited a high Cs of 1876 C·g^{-1} at 5 mA·cm^{-2} and a capacitance retention of 83.1% over 1000 cycles at 25 mA·cm^{-2}. The performance depended on its structure. In the composite structure, $Co(OH)_2$ nanosheets could grow both in space and on top of the Co_3O_4 nanotubes. In addition, a $Co_3O_4/Ni(OH)_2$ nanosheet core–shell electrode material was directly grown on the surface of NF substrate [160]. Due to the unique properties of 2D nanomaterials, $Co_3O_4/Ni(OH)_2$ electrode material effectively increased the active surface reaction with the electrolyte and facilitated ion diffusion. It displayed a high Cs of 1306.3 F·g^{-1} at 1.2 A·g^{-1}, a capacitance retention of approximately 90% after 3000 cycles, and a capacity retention of about 46% at 12 A·g^{-1}. The assembled $Co_3O_4/Ni(OH)_2$//AC solid-state asymmetric SC exhibited an E of 40 Wh·kg^{-1} at a P of 3455 W·kg^{-1}.

Through a large number of investigations, it was found that the performance of hydroxide electrode materials with a single metal element could not meet the actual needs in many aspects. [161] Therefore, two or more metal elements of hydroxides were often combined to achieve complementary advantages. For example, a core–shell nanosheet structural Co_3O_4/CoNi-layered double hydroxide (LDH) electrode material was deposited on NF via the growth of a nanoplate CoNi-LDH shell on the surface of the Co_3O_4 core (Figure 12b) [162]. It exhibited a high Cs of 2676.9 F·g^{-1} at 0.5 A·g^{-1} and a capacitance retention of 67.7% after 10,000 cycles at 30 A·g^{-1}. The assembled asymmetric Co_3O_4/CoNi-LDH//AC device showed a high E of 61.23 Wh·kg^{-1} at a P of 750 W·kg^{-1}. In addition, a family of layered double hydroxide nanosheet (IML; I = Ni, Co; M = Mn, Co, Al, L = LDH) coated Co_3O_4 nanowire arrays on NF was prepared via the hydrothermal method following the in situ growth method (Figure 12c) [163]. The LDH electrode material was expanded in interplanar spacing by the glucose molecule intercalation. Benefiting from the structure of Co_3O_4/IML, the Co_3O_4/NiMn-LDH electrode material exhibited an excellent Cs of 1644 F·g^{-1} at 1 A·g^{-1} and a cycling stability of 94.2% after 5000 cycles. The assembled Co_3O_4/NiMn-LDH//AC asymmetric SC device showed an E of 38.4 W h·kg^{-1} at a P of 800 W·kg^{-1}. In addition to binary metal hydroxides, a core–shell structured Co_3O_4/NiCoAl-LDH hybrid electrode material was synthesized via the two-step hydrothermal method (Figure 12d) [164]. The Co_3O_4/NiCoAl-LDH nanowire electrode material exhibited a high Cs of 1104 F·g^{-1} at 1 A·g^{-1}, a rate capability of 663 F·g^{-1} at 20 A·g^{-1}, and a capacitance retention of 87.3% over 5000 cycles.

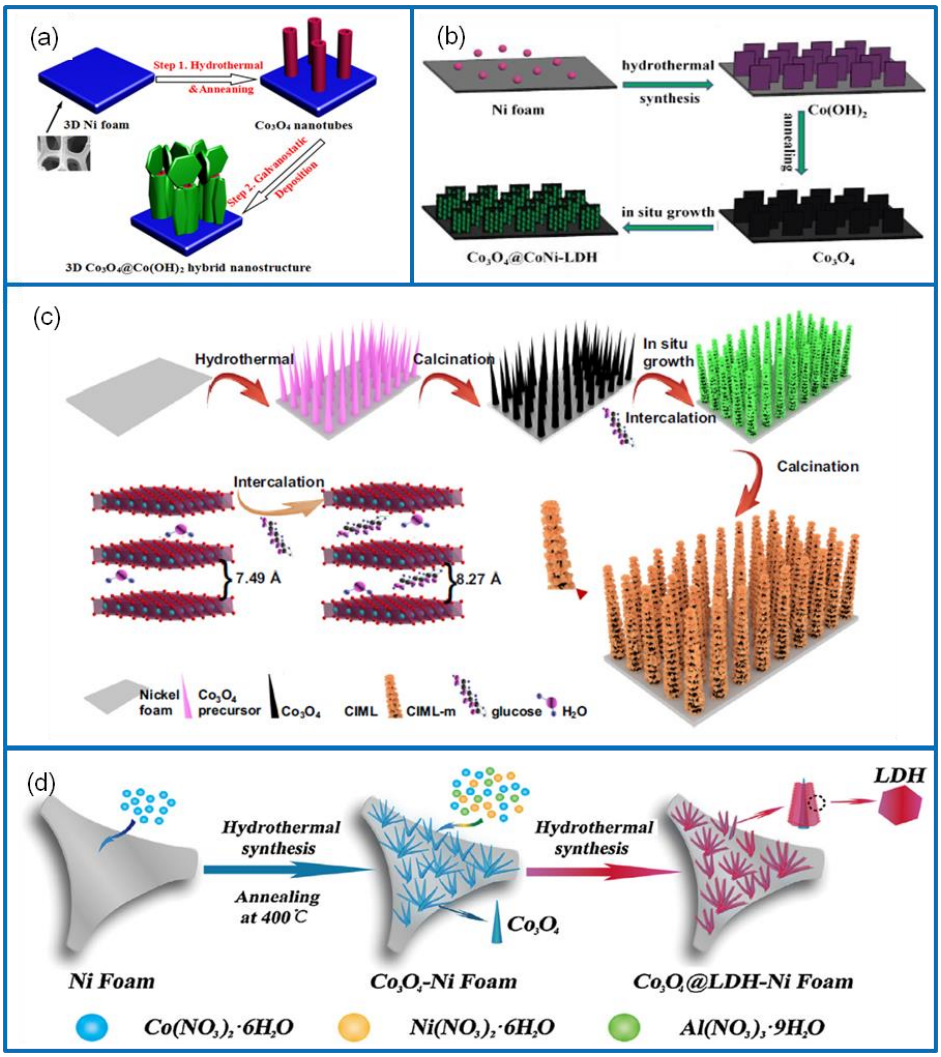

Figure 12. (**a**) Schematic route to synthesize 3D nonstructural Co_3O_4/$Co(OH)_2$ electrode material [159]. (**b**) Schematic illustration of preparing Co_3O_4/CoNi-layered double hydroxide (LDH) nanowire electrode material [162]. (**c**) Schematic illustration of preparing the Co_3O_4/IML electrode materials and expanding interplanar spacing by the glucose molecule intercalation [163]. (**d**) Fabrication of the core–shell structural Co_3O_4/NiCoAl-LDH hybrid electrode material [164].

3.3.4. Co_3O_4/Metal Sulfide Composites

Metal sulfide is considered to be a potentially high-performance electrode material, such as CoS, Co_3S_4, Ni_3S_2, CdS, Cu_2S, and Ag_2S [165]. Due to its low cost, high conductivity, mechanical property, and electrochemical activity, metal sulfide has become a kind of popular electrode material for Cs. Moreover, it has a rich redox reaction valence state, which helps with obtaining a high Cs. For the Co_3O_4 composite, 3D core–shell Co_3O_4/CoS nanosheet arrays were prepared on CC via the two-step electrodeposition method (Figure 13a) [166]. It exhibited a Cs of 764.2 $F{\cdot}g^{-1}$ at 1 $A{\cdot}g^{-1}$, a rate retention of 72.2% at 10 $A{\cdot}g^{-1}$, and a capacitance retention of 78.1% after 5000 cycles at 5 $A{\cdot}g^{-1}$. At the same time, Yan et al. [167] synthesized another Co_3S_4/Co_3O_4 core–shell structure with a different Co/S ratio via the hydrothermal lattice anion exchange method. The composite showed a Cs of 899 $F{\cdot}g^{-1}$ at 4 $A{\cdot}g^{-1}$ and a capacitance retention of 89.6% after 10,000 cycles. Further, a 3D core–shell of Co_3O_4/Ni_3S_2 nanowire electrode material was fabricated on NF via the hydrothermal method following electrodeposition [168]. It exhibited a high Cs of 1710 $F{\cdot}g^{-1}$ at 1 $A{\cdot}g^{-1}$, a rate capability capacitance of 86.2% at 10 $A{\cdot}g^{-1}$, and a capacitance retention of 85.3% after 1000 cycles. The assembled asymmetric Co_3O_4/Ni_3S_2//AC SC

device showed a Cs of 126.6 $F \cdot g^{-1}$ at 1 $A \cdot g^{-1}$, a retention capacity of 88.5% over 5000 cycles, and a high E of 44.9 $Wh \cdot kg^{-1}$ at a P of 798 $W \cdot kg^{-1}$.

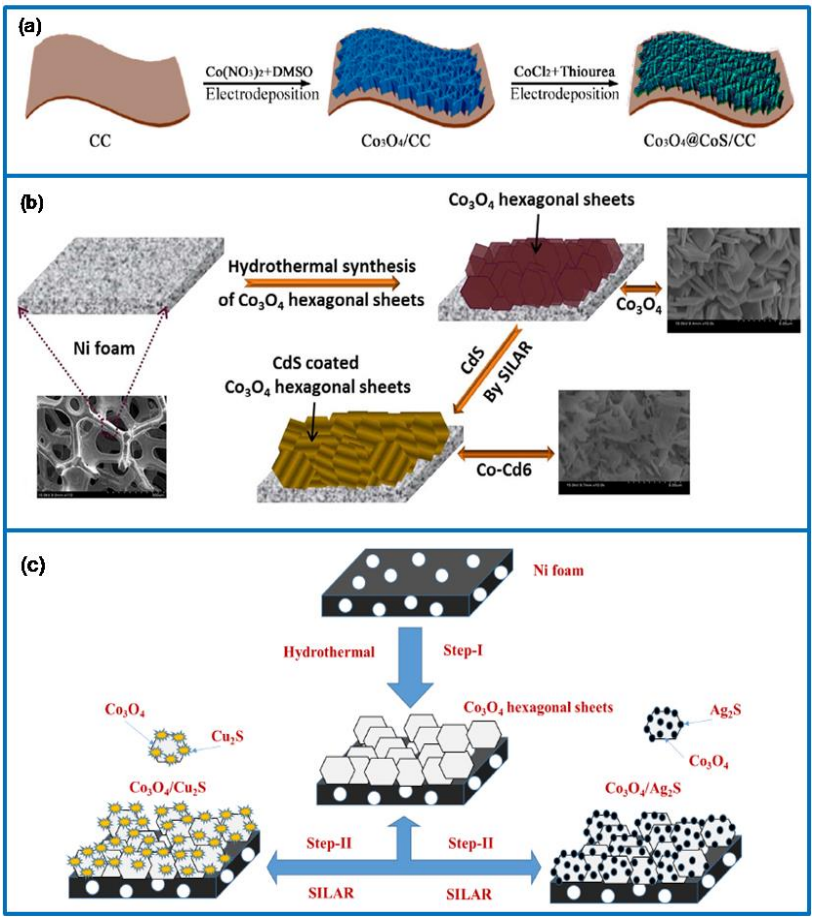

Figure 13. (**a**) Synthesis process of Co_3O_4/CoS nanosheet arrays on CC [166]. (**b**) Schematic illustration of preparing Co_3O_4/CdS on nickel foam (NF) [169]. (**c**) Schematic route to synthesize 3D Co_3O_4/Cu_2S and Co_3O_4/Ag_2S electrode materials [170].

In addition, a core–shell Co_3O_4/CdS nanostructure was prepared on NF via the hydrothermal method following the ionic layer adsorption and reaction (ILAR) method (Figure 13b) [169]. It exhibited a high Cs of 1539 $F \cdot g^{-1}$ at 10 $mV \cdot s^{-1}$ and a capacitance retention of 98.5% after 2000 cycles. The symmetric Co_3O_4/CdS//Co_3O_4/CdS SC device displayed a Cs of 360 $F \cdot g^{-1}$ at 10 $mV \cdot s^{-1}$, a capacitance retention of 92% after 2000 cycles, and a high E of 40 $Wh \cdot kg^{-1}$ at 10 mA. Recently, 3D Cu_2S and Ag_2S metal sulfides combined Co_3O_4 nanostructure electrode materials were synthesized via the one-pot approach followed by the ILAR method (Figure 13c) [170]. The resulting 3D Co_3O_4/Cu_2S and Co_3O_4/Ag_2S electrode materials offered a highly conductive network, which achieved a quick transfer of ions and electrons and reduced internal resistance. The Co_3O_4/Cu_2S electrode material exhibited an areal capacitance of 5324 $mF \cdot cm^{-2}$ at 10 $mV \cdot s^{-1}$, a good rate capability of 1630 $mF \cdot cm^{-2}$ at 100 $mV \cdot s^{-1}$, and a capacitance retention of 98.2% after 2000 cycles. Meanwhile, the Co_3O_4/Ag_2S composite showed an areal capacitance of 2243 $mF \cdot cm^{-2}$ at 10 $mV \cdot s^{-1}$, a rate capability of 966 $mF \cdot cm^{-2}$ at 100 $mV \cdot s^{-1}$, and a capacitance retention of 96.7% after 2000 cycles. When they were assembled in a symmetrical SCs, the Co_3O_4/Cu_2S//Co_3O_4/Cu_2S electrode exhibited an areal capacitance of 1080 $mF \cdot cm^{-2}$ and a capacitance retention of 93.2% after 2000 cycles, while the Co_3O_4/Ag_2S//Co_3O_4/Ag_2S SC showed an areal capacitance of 645 $mF \cdot cm^{-2}$ and a capacitance retention of 92.8% over 2000 cycles.

3.4. Co_3O_4/Multiple Materials Composites

In addition to the above binary composites containing Co_3O_4, multiple-component materials containing Co_3O_4 have already been extensively reported [171–175]. Due to the synergistic effect of multiple components, the unique interfacial structure in multiple-component materials ensures an excellent electrochemical performance. A tremelliform Co_3O_4/NiO/Mn_2O_3 material was prepared via the template method [176]. It exhibited a high Cs of 3652 mF·cm^{-2} at 1 mA·cm^{-2}, a rate property of 70% at 20 mA·cm^{-2}, and a capacitance retention of 87.6% after 10,000 cycles. The performance was much better than that of Co_3O_4/NiO and Co_3O_4/Mn_2O_3. Moreover, asymmetrical Co_3O_4/NiO/Mn_2O_3//rGO SC showed a high E of 65.7 Wh·kg^{-1} at a P of 343.4 W·kg^{-1} within a voltage window of 1.7 V and a capacitance retention of 82% after 5000 cycles at 10 mA·cm^{-2}. A hollow polyhedral network-like Co_3O_4/$NiCo_2O_4$/$ZnCo_2O_4$ electrode material was prepared via the coprecipitation and template method (Figure 14a) [177]. It exhibited a high Cs of 1892.5 F·g^{-1} at 1 A·g^{-1}, a rate capacitance of 1135 F·g^{-1} at 10 A·g^{-1}, and a capacitance retention of 66% over 2000 cycles. The assembled Co_3O_4/$NiCo_2O_4$/$ZnCo_2O_4$//AC SC device delivered a Cs of 233.75 F·g^{-1} at 1 A·g^{-1}, a capacitance retention of 92% over 3000 cycles, and a high E of 83.11 Wh·kg^{-1} at a P of 800 W·kg^{-1}. Additionally, a multielement Co_3O_4/C/MnO_2 heterostructure on NF was prepared via a stepwise method (Figure 14b) [178]. It delivered a high Cs of 1561.3 F·g^{-1} at 0.5 A·g^{-1}, a rate capability of 1335.3 F·g^{-1} at 20 A·g^{-1}, and a capacitance retention of 95% over 10,000 cycles. Compared with its counterpart, the improved performance was attributed to the synergistic effect between multicomponents and C, which promoted the electron transfer between MnO_2 and Co_3O_4.

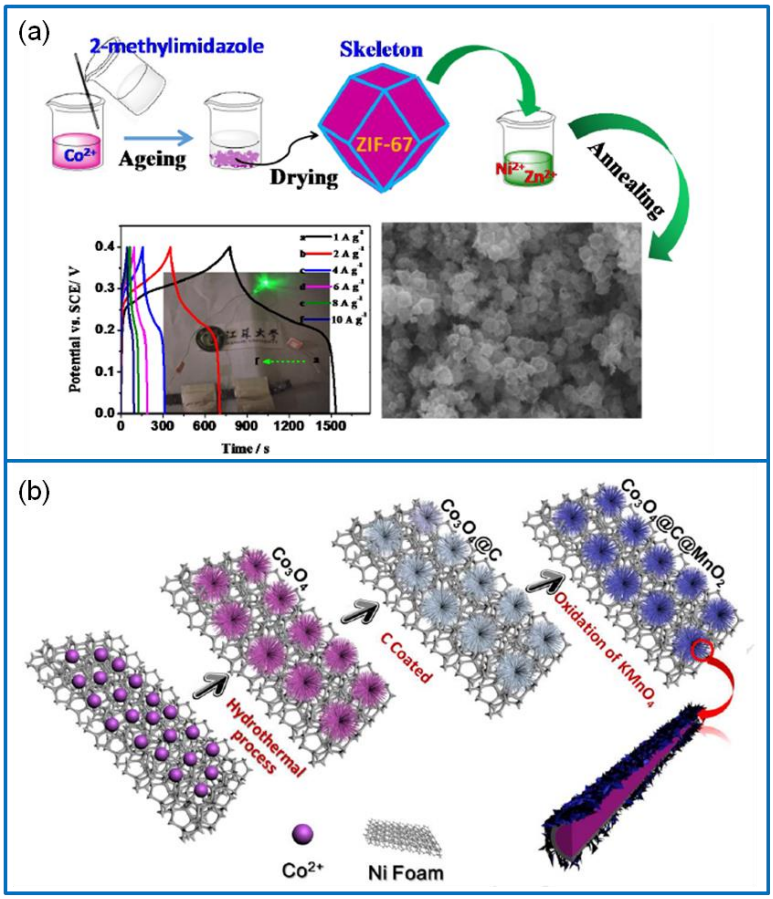

Figure 14. (**a**) Schematic route to synthesize the hollow polyhedral network-like Co_3O_4/$NiCo_2O_4$/$ZnCo_2O_4$ composite [177]. (**b**) Fabrication of the heterostructural Co_3O_4/C/MnO_2 electrode material [178].

Further, a high performance Co_3O_4/CNT/SS electrode material was fabricated via the electrodeposition method [179]. By adding SS core as a flow collector to CNT, the conductivity and electrodeposition efficiency of Co_3O_4 electrode were greatly improved. On the basis of these merits, the Co_3O_4/CNT/SS electrode material showed a volumetric capacitance of 82.94 F·cm^{-3} at 0.02 V·s^{-1} and an E of 1.31 mWh·cm^{-3} at a P of 294.80 mW·cm^{-3}. Recently, a freestanding and flexible Co_3O_4-PPy-rGO electrode material was synthesized via hydrothermal, thermal reduction, and the electrochemical deposition method [180]. It exhibited a Cs of 532.8 F·g^{-1} at 5 mV·s^{-1} and a capacitance retention of 100% after 700 cycles. Due to the synergistic effect of Co_3O_4, PPy, and RGO, the electrochemical performance was much better than that of a single component. Among the electrode materials, Co_3O_4 nanoparticles and PPy were used to improve capacitance and reduce resistance. The rGO nanosheet could provide a large surface area. In addition, a multicomponent Co_3O_4/$NiCo_2O_4$/NiO/C&S composite was fabricated via the solvothermal and thermal decomposition method [181]. It showed an ultralong cycling retention of 94.2% after 20,000 cycles at 3 A·g^{-1}. This excellent performance was attributed to the synergies among multicomponents and the highly stable structure formed by incompletely carbonized C and vulcanized S.

3.5. Performance Comparison of Co_3O_4-Containing Composites

The electrochemical performance of Co_3O_4-containing composites is summarized in Table 2. In general, compared with Co_3O_4, the performance of Co_3O_4-containing composites has been improved greatly, such as through high Cs, a long cycling stability, and a high rate capability. This performance is related to the morphology, stability, and Co_3O_4 nanoarrays on conductive substrates. Various Co_3O_4 structures have been reported, including nanosheet, nanowire, nanorod, and nanoparticle shapes. Moreover, a high surface area and more active sites of the Co_3O_4 composite are also required. For example, the Co_3O_4/PANI [113] electrode composite increased the contact between electrode and electrolyte for a high surface area, which is extremely helpful in improving the Cs. As for improving the rate performance and cycling stability of Co_3O_4 composites, the design and preparation of Co_3O_4 nanoarrays on conductive substrates is an important pathway. The core–shell Co_3O_4@MnO_2 [135] nanoarrays are a good example. As a result, the contact area between the Co_3O_4 nanoarrays and the electrolyte increases. This is favorable for the infiltration of electrolytes with relatively low internal resistance. The Co_3O_4 nanoarray can be directly combined with conductive substrate, which facilitates the transfer of electrons, shortens the distance of electron/ion migration, and enhances mechanical stability. Therefore, low internal resistance and high electrochemical stability will lead to a high-rate performance and cycling stability. In addition, the synergistic effect of different components in composites is much more important. The Co_3O_4/C/MnO_2 [178] composite delivered a better electrochemical performance. The electrical conductivity of Co_3O_4/C/MnO_2 was improved through the introduction of C. The synergistic effect of the MnO_2 nanosheet shell on lily-like nanostructures Co_3O_4 core could promote electron transfer and reduce the impedance and ion diffusion resistance of electrolytes. In addition, the Co_3O_4 nanostructure can be used as a better support and template to obtain composites with three-dimensional porous topology.

Table 2. Electrochemical performance of Co_3O_4-containing electrode materials.

Materials	Co_3O_4 Structure	Specific Capacitance	Rate	Cycle life Retention	Ref.
Co_3O_4/SWCNT	Porous nanoflake	313.9 $F{\cdot}g^{-1}$ at 1 $mV{\cdot}s^{-1}$	39.6% at 20 $mV{\cdot}s^{-1}$	80% after 3000 cycles	[78]
Co_3O_4/MWCNT	Nanofiber	406 $F{\cdot}g^{-1}$ at 2 $A{\cdot}g^{-1}$	41.9% at10 $A{\cdot}g^{-1}$	93% after 10,000 cycles	[80]
Co_3O_4/CF	Nanoparticle	586 $F{\cdot}g^{-1}$ at 1 $A{\cdot}g^{-1}$	66% at 50 $A{\cdot}g^{-1}$	74% after 2000 cycles	[83]
Co_3O_4/CF	Nanoparticle	948.9 $F{\cdot}g^{-1}$ at 0.5 $A{\cdot}g^{-1}$	48.2% at 40 $A{\cdot}g^{-1}$	88% after 6000 cycles	[85]
Co_3O_4/AC	Nanoparticle	491 $F{\cdot}g^{-1}$ at 0.1 $A{\cdot}g^{-1}$	82% at 5 $A{\cdot}g^{-1}$	89% after 5000 cycles	[91]
Co_3O_4/TC	Nanoparticle	885 $F{\cdot}g^{-1}$ at 2.5 $A{\cdot}g^{-1}$	23.7% at 20 $A{\cdot}g^{-1}$	94% over 10,000 cycles	[96]
Co_3O_4/CA	Ultrafine nanoparticle	616 $F{\cdot}g^{-1}$ at 1 $A{\cdot}g^{-1}$	72.2% at 20 $A{\cdot}g^{-1}$	93.6% after 5000 cycles	[100]
Co_3O_4/CA	Nanowire	1167.6 $F{\cdot}g^{-1}$ at 1 $A{\cdot}g^{-1}$	42.8% at 50 $A{\cdot}g^{-1}$	92.4% after 10,000 cycles	[101]
Co_3O_4/grapheme	Nanofiber	1935 $F{\cdot}g^{-1}$ at 1 $A{\cdot}g^{-1}$	72.9% at 50 $A{\cdot}g^{-1}$	83% after 2000 cycles	[34]
Co_3O_4/grapheme	Flower-like microsphere	1625.6 $F{\cdot}g^{-1}$ at 0.5 $A{\cdot}g^{-1}$	-	87% after 5000 cycles	[108]
Co_3O_4/PANI	Spherical nanoparticle	1184 $F{\cdot}g^{-1}$ at 1.25 $A{\cdot}g^{-1}$	42.2% at 50 $A{\cdot}g^{-1}$	84.9% after 1000 cycles	[113]
Co_3O_4/PANI	Nanocage particle	1301 $F{\cdot}g^{-1}$ at 1 $A{\cdot}g^{-1}$	62.6% at 10 $A{\cdot}g^{-1}$	90% after 2000 cycles	[114]
Co_3O_4/PPy	Nanowire	2122 $F{\cdot}g^{-1}$ at 5 $mA{\cdot}cm^{-2}$	53.3% at 50 $mA{\cdot}cm^{-2}$	77.8% after 5000 cycles	[118]
Co_3O_4/PPy	Nanorod	6.67 $F{\cdot}cm^{-2}$ at 2 $mA{\cdot}cm^{-2}$	97.4% at 20 $mA{\cdot}cm^{-2}$	~100% after 2000 cycles	[120]
Co_3O_4/PEDOP	Nanorod	582 $F{\cdot}g^{-1}$ at 0.5 $A{\cdot}g^{-1}$	69.9% at 1 $A{\cdot}g^{-1}$	78% after 5000 cycles	[122]
Co_3O_4/Pind	Nanoparticle	1805 $F{\cdot}g^{-1}$ at 2 $A{\cdot}g^{-1}$	90% at 25 $A{\cdot}g^{-1}$	85% after 1000 cycles	[123]
Co_3O_4/NiO	Nanorod	313.9 $\mu Ah{\cdot}cm^{-2}$ at 4 $mA{\cdot}cm^{-2}$	76.38% at 25 $mA{\cdot}cm^{-2}$	135% after 2000 cycles	[131]
Co_3O_4/ZnO	Flower-like nanobundle	1983 $F{\cdot}g^{-1}$ at 2 $A{\cdot}g^{-1}$	42% at 20 $A{\cdot}g^{-1}$	84.5% after 5000 cycles	[132]
Co_3O_4/CuO	Nanowire	1242 $F{\cdot}g^{-1}$ at 2 $mV{\cdot}s^{-1}$	51% at 50 $mV{\cdot}s^{-1}$	100% after 2000 cycles	[133]
Co_3O_4/CoO	Nanomicrosphere	3377.8 $F{\cdot}g^{-1}$ at 2 $A{\cdot}g^{-1}$	66.5% at 20 $A{\cdot}g^{-1}$	39.4% after 4000 cycles	[134]
Co_3O_4/MnO_2	Nanowire	1920 $F{\cdot}g^{-1}$ at 1 $A{\cdot}g^{-1}$	-	95.2% after 3000 cycles	[135]
Mn-doping Co_3O_4	Nanoneedle	668.4 $F{\cdot}g^{-1}$ at 1 $A{\cdot}g^{-1}$	61.7% at 10 $A{\cdot}g^{-1}$	104% after 10,000 cycles	[155]
Fe-doping Co_3O_4	Flowerlike nanoflake	1997 $F{\cdot}g^{-1}$ at 1 $A{\cdot}g^{-1}$	61.7% at 20 $A{\cdot}g^{-1}$	92.1% after 5000 cycles	[138]
Co_3O_4/$NiCo_2O_4$	Nanosheet	1330 $F{\cdot}g^{-1}$ at 3 $mA{\cdot}cm^{-2}$	72.2% at 30 $mA{\cdot}cm^{-2}$	100.7% over 5000 cycles	[150]
Co_3O_4/$NiMoO_4$	Nanofiber	998.05 $F{\cdot}g^{-1}$ at 0.5 $A{\cdot}g^{-1}$	88% at 20 $A{\cdot}g^{-1}$	89.9% after 3000 cycles	[151]
Co_3O_4/$CoWO_4$	Nanocone	4.665 $F{\cdot}cm^{-2}$ at 2.7 $mA{\cdot}cm^{-2}$	70.83% at 27 $mA{\cdot}cm^{-2}$	-	[152]

Table 2. *Cont.*

Materials	Co_3O_4 Structure	Specific Capacitance	Rate	Cycle life Retention	Ref.
$Co_3O_4/ZnFe_2O_4$	Nanocage particle	326.7 $F{\cdot}g^{-1}$ at 1 $A{\cdot}g^{-1}$	51.8% at 10 $A{\cdot}g^{-1}$	80.7% after 1000 cycles	[153]
$Co_3O_4/CoFe_2O_4$	Nanoparticle	761.1 $F{\cdot}g^{-1}$ at 10 $mV{\cdot}s^{-1}$	20.9% at 50 $mV{\cdot}s^{-1}$	92.2% after 1000 cycles	[154]
$Co_3O_4/CoMn_2O_4$	Nanosheet	1627 $F{\cdot}g^{-1}$ at 1 $A{\cdot}g^{-1}$	84.6% at 10 $A{\cdot}g^{-1}$	87.6% over 3000 cycles	[155]
$Co_3O_4/MnCo_2O_4$	Polyhedron nanoparticle	1440 $C{\cdot}cm^{-2}$ at 1 $mA{\cdot}cm^{-2}$	36% at 10 $mA{\cdot}cm^{-2}$	82.76% after 8000 cycles	[156]
$Co_3O_4/Co(OH)_2$	Nanotube	1876 $C{\cdot}g^{-1}$ at 5 $mA{\cdot}cm^{-2}$	25.4% at 25 $mA{\cdot}cm^{-2}$	83.1% over 1000 cycles	[159]
$Co_3O_4/Ni(OH)_2$	Nanosheet	1306.3 $F{\cdot}g^{-1}$ at 1.2 $A{\cdot}g^{-1}$	46% at 12 $A{\cdot}g^{-1}$	90% after 3000 cycles	[160]
Co_3O_4/CoNi-LDH	Nanoplate	2676.9 $F{\cdot}g^{-1}$ at 0.5 $A{\cdot}g^{-1}$	43% at 20 $A{\cdot}g^{-1}$	67.7% after 10,000 cycles	[162]
Co_3O_4/NiMn-LDH	Nanowire	1644 $F{\cdot}g^{-1}$ at 1A$\cdot g^{-1}$	42.4% at 10A$\cdot g^{-1}$	94.2% after 5000 cycles	[163]
Co_3O_4/CoS	Nanosheet	764.2 $F{\cdot}g^{-1}$ at 1.0 $A{\cdot}g^{-1}$	72.2% at 10 $A{\cdot}g^{-1}$	78.1% after 5000 cycles	[166]
Co_3O_4/Ni_3S_2	Nanowire	1710 $F{\cdot}g^{-1}$ at 1A$\cdot g^{-1}$	86.2% at 10 $A{\cdot}g^{-1}$	85.3% after 1000 cycles	[168]
Co_3O_4/CdS	Nanosheet	1539 $F{\cdot}g^{-1}$ at 10$mV{\cdot}s^{-1}$	52% at 100 $mV{\cdot}s^{-1}$	98.5% after 2000 cycles	[169]
Co_3O_4/Cu_2S	Nanosheet	5324 $mF{\cdot}cm^{-2}$ at 10 $mV{\cdot}s^{-1}$	30.6% at 100 $mV{\cdot}s^{-1}$	98.2% after 2000 cycles	[170]
Co_3O_4/Ag_2S	Nanosheet	2243 $mF{\cdot}cm^{-2}$ at 10 $mV{\cdot}s^{-1}$	43.1% at 100 $mV{\cdot}s^{-1}$	96.7% after 2000 cycles	[170]
Co_3O_4/NiO/Mn_2O_3	Nanosheet	3652 $mF{\cdot}cm^{-2}$ at 1 $mA{\cdot}cm^{-2}$	70% at 20 $mA{\cdot}cm^{-2}$	87.6% after 10,000 cycles	[176]
$Co_3O_4/NiCo_2O_4$/ $ZnCo_2O_4$	Nanocage particle	1892.5 $F{\cdot}g^{-1}$ at 1 $A{\cdot}g^{-1}$	60% at 10 $A{\cdot}g^{-1}$	66% after 2000 cycles	[177]
Co_3O_4/C/MnO_2	Lily-like nanostructures	1561.3 $F{\cdot}g^{-1}$ at 0.5 $A{\cdot}g^{-1}$	85.5% at 20 $A{\cdot}g^{-1}$	95% after 10,000 cycles	[178]
Co_3O_4/CNT/SS	Nanoparticle	82.94 $F{\cdot}cm^{-3}$ at 0.02 $V{\cdot}s^{-1}$	58.96 at 0.05 $V{\cdot}s^{-1}$	80.4 after 1000 cycles	[179]
Co_3O_4-PPy-rGO	Nanoparticle	532.8 $F{\cdot}g^{-1}$ at 5 $mV{\cdot}s^{-1}$	-	100% after 700 cycles	[180]
$Co_3O_4/NiCo_2O_4$/ NiO/C&S	Nanoparticle	428.24 $F{\cdot}g^{-1}$ at 0.5 $A{\cdot}g^{-1}$	61.5% at 10 $A{\cdot}g^{-1}$	94.2% after 20,000 cycles	[181]

4. Conclusions and Perspective

4.1. Conclusions

In summary, we have presented the recent progress on Co_3O_4 and Co_3O_4-containing electrode materials for high-performance SCs. Various synthetic methods and the electrochemical performance of Co_3O_4 electrode materials are summarized. The electrochemical performance of Co_3O_4 is compared according to the synthetic methods. Among these methods, solvothermal is the one most commonly used to synthesize Co_3O_4 electrode materials. Because the Co_3O_4 nanoparticles synthesized via the solvothermal method have a smaller size and a larger specific surface area, they offer more active sites. However, more and more researchers are paying attention to the template method. Compared to the solvothermal method, the template method can be used to design and synthesize Co_3O_4 nanomaterials. The products have the same morphology and size as the template. We can perfectly synthesize Co_3O_4

with a certain nanomorphology and pore structure, which increases the contact between electrode and electrolyt, and facilitates the charge transfer. For instance, Co_3O_4 electrode materials with ultrathin nanosheets often show a high electrochemical performance.

For Co_3O_4-containing electrode materials, we introduced the candidate hybrid materials, including carbon, conductive polymer, and metal compound materials. The multiple composites show better electrochemical performance due to the synergistic effect of several components, which effectively improve the Cs, E, P, cycling stability, and rate capacity of SCs. To date, Co_3O_4/graphene composites are the hottest research topic in SCs. Further, the composites consisting of Co_3O_4 and conductive polymers exhibited an excellent electrochemical performance, which is due to the easy diffusion of electrons and ions in conductive polymers. In addition, the abundant active sites in conductive polymers also facilitate the diffusion of electrolytes. In recent years, Co_3O_4/ternary metal oxide and Co_3O_4/metal sulfide composites have become the research focus. So far, SCs have been used in all aspects of society and have become an indispensable energy storage device. The wide application puts forward a high requirement for the specific capacitance and specific energy. Therefore, the design and development of Co_3O_4 and Co_3O_4-containing composites are urgently required to further improve the performance of SCs.

4.2. Perspective

Although great progress has been achieved in Co_3O_4 and Co_3O_4-containing electrode materials, there are still some problems to be solved in the application for SCs, such as the big gap between actual and theoretical specific capacitance, poor electrical conductivity, lower specific energy, and unclear development direction of Co_3O_4 and Co_3O_4-containing electrode materials. In order to solve these problems, some suitable strategies are put forward as follows:

(1) Designing Co_3O_4 and Co_3O_4-containing electrode materials with a high specific surface area and abundant porous structure. The large active surface of electrode materials is beneficial to electrolyte contact and adsorption of ions, which can decrease the electrolyte starvation near the electrode surface and facilitate ionic diffusion in the electrode. The unique porous structure ensures an efficient Faradaic reaction from outside to inside, leading to capacitance improvement. Therefore, a suitable synthesis method is urgently needed to control the specific morphology and structure of Co_3O_4 and Co_3O_4-containing electrode materials.

(2) Hybridizing Co_3O_4 with conductive materials, including PANI, PPy, CNT, graphene, etc. The candidate materials should be considered to enhance the conductive feature of Co_3O_4, so as to improve the rate performance and cycling stability of Co_3O_4-containing composites. Meanwhile, the ordered Co_3O_4 nanoarrays provide a large surface area and short diffusion path for ion transfer, which will contribute much more pseudocapacitance.

(3) Developing novel Co_3O_4 and Co_3O_4-containing electrode materials. Novel structures and morphologies depend on the synthesis methods and synthesis conditions. Therefore, the development of various Co_3O_4 microstructures is still an important task. In terms of hybridization, we should continuously explore suitable substances and make use of the synergistic effects between multiple substances to further improve the electrochemical performance of Co_3O_4.

(4) Enlarging the working voltage window of the Co_3O_4 and Co_3O_4-containing electrode materials. In addition to increasing capacitance, enlarging operating voltage is also an effective way to increase specific energy. Due to the easy decomposition and narrow voltage window of aqueous electrolytes, organic electrolytes, ionic liquids, and solid-state/gel electrolytes should be considered to expand the working voltage window, so as to improve the specific energy of Co_3O_4 and Co_3O_4-containing composites.

Author Contributions: X.W. contributed to writing the article. X.H. contributed to designing the article. A.H., C.M., C.W., and S.Y. contributed critical revisions to the article and intellectual discussions. All authors have read and agreed to the published version of the manuscript.

Funding: This work is supported by the National Natural Science Foundation of China (51805235, 51774175, 51403094), the Department of Education of Liaoning Province (LJ2017QL005), Liaoning Province-Shenyang National Research Center for Materials Science Joint R&D Fund Project (1572573319971), and College Students' innovation training program (201810147077).

Conflicts of Interest: The authors declare no conflict of interest.

References

1. Zhao, M.M.; Zhao, Q.X.; Li, B.; Xue, H.G.; Pang, H.; Chen, C.Y. Recent progress in layered double hydroxide based materials for electrochemical capacitors: Design, synthesis and performance. *Nanoscale* **2017**, *9*, 15206–15225. [CrossRef] [PubMed]
2. Winter, M.; Brodd, R.J. What are batteries, fuel cells, and supercapacitors? *Chem. Rev.* **2004**, *104*, 4245–4270. [CrossRef]
3. Kasnatscheew, J.; Wagner, R.; Winter, M.; Cekic-Laskovic, I. Interfaces and Materials in Lithium Ion Batteries: Challenges for Theoretical Electrochemistry. In *Modeling Electrochemical Energy Storage at the Atomic Scale*; Springer: Münster, Germany, 2018; pp. 23–51.
4. Miller, J.R. Reliability of Electrochemical Capacitors. In *Supercapacitors: Materials, Systems, and Applications*; Wiley-VCH: Weinheim, Germany, 2013; Chapter 13; pp. 473–507.
5. Wang, Y.; Guo, J.; Wang, T.; Shao, J.; Wang, D.; Yang, Y.W. Mesoporous Transition Metal Oxides for Supercapacitors. *Nanomaterials* **2015**, *5*, 1667–1689. [CrossRef] [PubMed]
6. Ujjain, S.K.; Singh, G.; Sharma, R.K. Co_3O_4@Reduced Graphene Oxide Nanoribbon for high performance Asymmetric Supercapacitor. *Electrochim. Acta* **2015**, *169*, 276–282. [CrossRef]
7. Guan, Q.; Cheng, J.; Wang, B.; Ni, W.; Gu, G.; Li, X.; Huang, L.; Yang, G.; Nie, F. Needle-like Co_3O_4 Anchored on the Graphene with Enhanced Electrochemical Performance for Aqueous Supercapacitors. *ACS Appl. Mater. Interfaces* **2014**, *6*, 7626–7632. [CrossRef] [PubMed]
8. Jiang, J.; Shi, W.; Song, S.; Hao, Q.; Fan, W.; Xia, X.; Zhang, X.; Wang, Q.; liu, C.; Yan, D. Solvothermal synthesis and electrochemical performance in super-capacitors of Co_3O_4/C flower-like nanostructures. *J. Power Sources* **2014**, *248*, 1281–1289. [CrossRef]
9. Liu, X.; Long, Q.; Jiang, C.; Zhan, B.; Li, C.; Liu, S.; Zhao, Q.; Huang, W.; Dong, X. Facile and green synthesis of mesoporous Co_3O_4 nanocubes and their applications for supercapacitors. *Nanoscale* **2013**, *5*, 6525–6529. [CrossRef]
10. Xiang, C.; Li, M.; Zhi, M.; Manivannan, A.; Wu, N. A reduced graphene oxide/Co_3O_4 composite for supercapacitor electrode. *J. Power Sources* **2013**, *226*, 65–70. [CrossRef]
11. Yuan, J.; Zhu, J.; Bi, H.; Meng, X.; Liang, S.; Zhang, L.; Wang, X. Graphene-based 3D composite hydrogel by anchoring Co_3O_4 nanoparticles with enhanced electrochemical properties. *Phys. Chem. Chem. Phys.* **2013**, *15*, 12940–12945. [CrossRef]
12. Zhang, Y.F.; Ma, M.Z.; Yang, J.; Sun, C.C.; Su, H.Q.; Huang, W.; Dong, X.C. Shape-controlled synthesis of $NiCo_2S_4$ and their charge storage characteristics in supercapacitors. *Nanoscale* **2014**, *6*, 9824–9830. [CrossRef]
13. Nithya, V.D.; Arul, N.S. Review on α-Fe_2O_3 based negative electrode for high performance supercapacitors. *J. Power Sources* **2016**, *327*, 297–318. [CrossRef]
14. Zhang, H.; Zhang, Y.; Gu, C.; Ma, Y. Electropolymerized Conjugated Microporous Poly(zinc-porphyrin) Films as Potential Electrode Materials in Supercapacitors. *Adv. Energy. Mater* **2015**, *5*, 1402175. [CrossRef]
15. Wang, J.; Zhang, Q.; Li, X.; Xu, D.; Wang, Z.; Guo, H.; Zhang, K. Three-dimensional hierarchical Co_3O_4/CuO nanowire heterostructure arrays on nickel foam for high-performance lithium ion batteries. *Nano Energy* **2014**, *6*, 19–26. [CrossRef]
16. Zhu, J.; Huang, L.; Xiao, Y.; Shen, L.; Chen, Q.; Shi, W. Hydrogenated CoOx nanowire@$Ni(OH)_2$ nanosheet core-shell nanostructures for high-performance asymmetric supercapacitors. *Nanoscale* **2014**, *6*, 6772–6781. [CrossRef]
17. Zhang, H.; Li, J.; Gu, C.; Yao, M.; Yang, B.; Lu, P.; Ma, Y. High performance, flexible, poly(3,4-ethylenedioxythiophene) supercapacitors achieved by doping redox mediators in organogel electrolytes. *J. Power Sources* **2016**, *332*, 413–419. [CrossRef]
18. Xiong, W.; Pan, X.; Li, Y.; Chen, X.; Zhu, Y.; Yang, M.; Zhang, Y. Hierarchical Co_3O_4@PPy core/shell nanowire arrays on nickel foam for electrochemical energy storage. *Mater. Lett.* **2015**, *157*, 23–26. [CrossRef]

19. Xu, H.; Hai, Z.; Diwu, J.; Zhang, Q.; Gao, L.; Cui, D.; Zang, J.; Liu, J.; Xue, C. Synthesis and microwave absorption properties of core-shell structured Co_3O_4-PANI nanocomposites. *J. Nanomater.* **2015**, *2015*, 9. [CrossRef]
20. Hong, X.; Lu, Y.; Li, S.; Wang, X.; Wang, X.; Liang, J. Carbon foam@reduced graphene oxide scaffold grown with polyaniline nanofibers for high performance symmetric supercapacitor. *Electrochim. Acta* **2019**, *294*, 376–382. [CrossRef]
21. Tang, C.H.; Yin, X.; Gong, H. Superior performance asymmetric supercapacitors based on a directly grown commercial mass 3D Co_3O_4@$Ni(OH)_2$ core-shell electrode. *ACS Appl. Mater. Interfaces* **2013**, *5*, 10574–10582. [CrossRef]
22. Deng, J.; Kang, L.; Bai, G.; Li, Y.; Li, P.; Liu, X.; Yang, Y.; Gao, F.; Liang, W. Solution combustion synthesis of cobalt oxides (Co_3O_4 and Co_3O_4/CoO) nanoparticles as supercapacitor electrode materials. *Electrochim. Acta* **2014**, *132*, 127–135. [CrossRef]
23. Huang, M.; Zhang, Y.; Li, F.; Zhang, L.; Wen, Z.; Liu, Q. Facile synthesis of hierarchical Co_3O_4@MnO_2 core–shell arrays on Ni foam for asymmetric supercapacitors. *J. Power Sources* **2014**, *252*, 98–106. [CrossRef]
24. Li, Y.; Zhang, Y.; Li, Y.; Wang, Z.; Fu, H.; Zhang, X.; Chen, Y.; Zhang, H.; Li, X. Unveiling the dynamic capacitive storage mechanism of Co_3O_4 @$NiCo_2O_4$ hybrid nanoelectrodes for supercapacitor applications. *Electrochim. Acta* **2014**, *145*, 177–184. [CrossRef]
25. Wang, X.F.; Liu, B.; Liu, R.; Wang, Q.F.; Hou, X.J.; Chen, D.; Wang, R.M.; Shen, G.Z. Fiber-Based Flexible All-Solid-State Asymmetric Supercapacitors for Integrated Photodetecting System. *Angew. Chem. Int. Ed.* **2014**, *53*, 1849–1853. [CrossRef]
26. Kong, D.Z.; Luo, J.S.; Wang, Y.L.; Ren, W.N.; Yu, T.; Luo, Y.S.; Yang, Y.P.; Cheng, C.W. Three-Dimensional Co_3O_4@MnO_2 Hierarchical Nanoneedle Arrays: Morphology Control and Electrochemical Energy Storage. *Adv. Funct. Mater* **2014**, *24*, 3815–3826. [CrossRef]
27. Yi, C.Q.; Zou, J.P.; Yang, H.Z.; Leng, X. A facile hydrothermal synthesis of graphene/RuO_2/Co_3O_4 nanocomposites with high pseudocapacity. *New J. Chem.* **2018**, *42*, 7066–7072. [CrossRef]
28. Gong, X.F.; Cheng, J.P.; Liu, F.; Zhang, L.; Zhang, X.B. Nickel-Cobalt hydroxide microspheres electrodepositioned on nickel cobaltite nanowires grown on Ni foam for high-performance pseudocapacitors. *J. Power Sources* **2014**, *267*, 610–616. [CrossRef]
29. Guo, J.X.; Chen, L.; Zhang, X.; Jiang, B.; Ma, L.Z. Sol–gel synthesis of mesoporous Co_3O_4 octahedra toward high-performance anodes for lithium-ion batteries. *Electrochim. Acta* **2014**, *129*, 410–415. [CrossRef]
30. Wang, Y.; Pan, A.; Zhu, Q.; Nie, Z.; Zhang, Y.; Tang, Y.; Liang, S.; Cao, G. Facile synthesis of nanorod-assembled multi-shelled Co_3O_4 hollow microspheres for high-performance supercapacitors. *J. Power Sources* **2014**, *272*, 107–112. [CrossRef]
31. Lee, M.; Wee, B.H.; Hong, J.D. High performance flexible supercapacitor electrodes composed of ultralarge graphene sheets and vanadium dioxide. *Adv. Energy Mater.* **2015**, *5*, 1401890. [CrossRef]
32. Ji, L.; Meduri, P.; Agubra, V.; Xiao, X.; Alcoutlabi, M. Graphene-Based Nanocomposites for Energy Storage. *Adv. Energy Mater.* **2016**, *6*, 1502159.
33. Yuan, K.; Xu, Y.; Uihlein, J.; Brunklaus, G.; Shi, L.; Heiderhoff, R.; Que, M.; Forster, M.; Chassé, T.; Pichler, T. Straightforward generation of pillared, microporous graphene frameworks for use in supercapacitors. *Adv. Mater.* **2015**, *27*, 6714–6721. [CrossRef] [PubMed]
34. Gao, Z.; Chen, C.; Chang, J.; Chen, L.; Wu, D.; Xu, F.; Jiang, K. Balanced energy density and power density: Asymmetric supercapacitor based on activated fullerene carbon soot anode and graphene-Co_3O_4 composite cathode. *Electrochim. Acta* **2018**, *260*, 932–943. [CrossRef]
35. Qiu, K.; Lu, Y.; Cheng, J.; Yan, H.; Hou, X.; Zhang, D.; Lu, M.; Liu, X.; Luo, Y. Ultrathin mesoporous Co_3O_4 nanosheets on Ni foam for high-performance supercapacitors. *Electrochim. Acta* **2015**, *157*, 62–68. [CrossRef]
36. Venkatachalam, V.; Alsalme, A.; Alswieleh, A.; Jayavel, R. Shape controlled synthesis of rod-like Co_3O_4 nanostructures as high-performance electrodes for supercapacitor applications. *J. Mater. Sci. Mater. El.* **2018**, *29*, 6059–6067. [CrossRef]
37. Wang, X.; Xia, H.; Wang, X.; Gao, J.; Shi, B.; Fang, Y. Facile synthesis ultrathin mesoporous Co_3O_4 nanosheets for high-energy asymmetric supercapacitor. *J. Alloys Compd.* **2016**, *686*, 969–975. [CrossRef]
38. Liu, F.; Zhang, B.; Su, H.; Zhang, H.; Zhang, L.; Yang, W. Controllable synthesis of self-assembly Co_3O_4 nanoflake microspheres for electrochemical performance. *Nanotechnology* **2016**, *27*, 355603. [CrossRef]

39. Jiang, Y.; Chen, L.; Zhang, H.; Zhang, Q.; Chen, W.; Zhu, J.; Song, D. Two-dimensional Co_3O_4 thin sheets assembled by 3D interconnected nanoflake array framework structures with enhanced supercapacitor performance derived from coordination complexes. *Chem. Eng. J.* **2016**, *292*, 1–12. [CrossRef]
40. Deori, K.; Ujjain, S.K.; Sharma, R.K.; Deka, S. Morphology controlled synthesis of nanoporous Co_3O_4 nanostructures and their charge storage characteristics in supercapacitors. *ACS Appl. Mater. Interfaces* **2013**, *5*, 10665–10672. [CrossRef]
41. Meng, T.; Xu, Q.Q.; Wang, Z.H.; Li, Y.T.; Gao, Z.M.; Xing, X.Y.; Ren, T.Z. Co_3O_4 Nanorods with Self-assembled Nanoparticles in Queue for Supercapacitor. *Electrochim. Acta* **2015**, *180*, 104–111. [CrossRef]
42. Liu, F.; Su, H.; Jin, L.; Zhang, H.; Chu, X.; Yang, W. Facile synthesis of ultrafine cobalt oxide nanoparticles for high-performance supercapacitors. *J. Colloid Interface Sci.* **2017**, *505*, 796–804. [CrossRef]
43. Liu, Z.Z.; Zhou, W.W.; Wan, S.S.; Du, W.; Zhang, H.L.; Ding, C.Y.; Du, Y.; Zhu, L.J. Facile synthesis of homogeneous core-shell Co_3O_4 mesoporous nanospheres as high performance electrode materials for supercapacitor. *J. Alloys Compd.* **2019**, *774*, 137–144. [CrossRef]
44. George, G.; Elias, L.; Hegde, A.C.; Anandhan, S. Morphological and structural characterisation of sol–gel electrospun Co_3O_4 nanofibres and their electro-catalytic behaviour. *RSC Adv.* **2015**, *5*, 40940–40949. [CrossRef]
45. Pudukudy, M.; Yaakob, Z. Sol–gel synthesis, characterisation, and photocatalytic activity of porous spinel Co_3O_4 nanosheets. *Chem. Pap.* **2014**, *68*, 1087–1096. [CrossRef]
46. Lima-Tenorio, M.K.; Ferreira, C.S.; Rebelo, Q.H.F.; de Souza, R.F.B.; Passos, R.R.; Pineda, E.A.G.; Pocrifka, L.A. Pseudocapacitance Properties of Co_3O_4 Nanoparticles Synthesized Using a Modified Sol–Gel Method. *Mater. Res* **2018**, *21*, e20170521. [CrossRef]
47. Lakehal, A.; Bedhiaf, B.; Bouaza, A.; Benhebal, H.; Ammari, A.; Dalache, C. Structural, optical and electrical properties of Ni-doped Co_3O_4 prepared via Sol–Gel technique. *Mater. Res* **2018**, *21*, e20170545. [CrossRef]
48. Peterson, G.R.; Hung-Low, F.; Gumeci, C.; Bassett, W.P.; Korzeniewski, C.; Hope-Weeks, L.J. Preparation–Morphology–Performance Relationships in Cobalt Aerogels as Supercapacitors. *ACS Appl. Mater. Interfaces* **2014**, *6*, 1796–1803. [CrossRef]
49. Farhadi, S.; Javanmard, M.; Nadri, G. Characterization of Cobalt Oxide Nanoparticles Prepared by the Thermal Decomposition of $Co(NH_3)_5(H_2O)(NO_3)_3$ Complex and Study of Their Photocatalytic Activity. *Acta Chim. Slov.* **2016**, *63*, 335–343. [CrossRef]
50. Xu, Y.N.; Ding, Q.; Li, L.; Xie, Z.J.; Jiang, G.X. Facile fabrication of porous Co_3O_4 nanowires for high performance supercapacitors. *New J. Chem.* **2018**, *42*, 20069–20073. [CrossRef]
51. Kong, S.Y.; Yang, F.; Cheng, K.; Ouyang, T.; Ye, K.; Wang, G.L.; Cao, D.X. In-situ growth of cobalt oxide nanoflakes from cobalt nanosheet on nickel foam for battery-type supercapacitors with high specific capacity. *J. Electroanal. Chem.* **2017**, *785*, 103–108. [CrossRef]
52. Lv, Y.N.; Dong, G.X.; Li, L.; Kang, J.R.; Han, W.D. Cobalt-Nickel Oxides with Three-Dimensional Hexagon Films for High Performance Supercapacitors. *Nano* **2018**, *13*, 1850032. [CrossRef]
53. Wang, D.; Wang, Q.; Wang, T. Morphology-controllable synthesis of cobalt oxalates and their conversion to mesoporous Co_3O_4 nanostructures for application in supercapacitors. *Inorg. Chem.* **2011**, *50*, 6482–6492. [CrossRef] [PubMed]
54. Wang, Y.; Lei, Y.; Li, J.; Gu, L.; Yuan, H.; Xiao, D. Synthesis of 3D-Nanonet Hollow Structured Co_3O_4 for High Capacity Supercapacitor. *ACS Appl. Mater. Interfaces* **2014**, *6*, 6739–6747. [CrossRef] [PubMed]
55. Song, F.M.; Zan, G.T.; Chen, Y.; Wu, Q.S.; Xu, Y.Y. In situ transformation of iron-group ternary metal oxides nanocubes from Co/Ni-PBA for high-performance supercapacitors. *J. Alloys Compd.* **2018**, *741*, 633–641. [CrossRef]
56. Meher, S.K.; Rao, G.R. Ultralayered Co_3O_4 for High-Performance Supercapacitor Applications. *J. Phys. Chem. C* **2011**, *115*, 15646–15654. [CrossRef]
57. Ren, S.R.; Guo, Y.K.; Ju, L.L.; Xiao, H.; Hu, A.M.; Li, M. Facile synthesis of petal-like nanocrystalline Co_3O_4 film using direct high-temperature oxidation. *J. Mater. Sci.* **2019**, *54*, 7922–7930. [CrossRef]
58. Aghazadeh, M.; Ahmadi, R.; Gharailou, D.; Ganjali, M.R.; Norouzi, P. A facile route to preparation of Co_3O_4 nanoplates and investigation of their charge storage ability as electrode material for supercapacitors. *J. Mater. Sci. Mater. El.* **2016**, *27*, 8623–8632. [CrossRef]

59. Guo, X.G.; Li, X.M.; Xiong, Z.S.; Lai, C.; Li, Y.; Huang, X.Y.; Bao, H.B.; Yin, Y.J.; Zhu, Y.H.; Zhang, D.X. A comprehensive investigation on electrophoretic self-assembled nano-Co_3O_4 films in aqueous solution as electrode materials for supercapacitors. *J. Nanopart. Res.* **2016**, *18*, 144. [CrossRef]
60. Pan, X.; Chen, X.; Li, Y.; Yu, Z. Facile Synthesis of Co_3O_4 Nanosheets Electrode with Ultrahigh Specific Capacitance for Electrochemical Supercapacitors. *Electrochim. Acta* **2015**, *182*, 1101–1106. [CrossRef]
61. Pan, G.X.; Xia, X.H.; Cao, E.; Chen, J.; Zhang, Y.J. Template-free synthesis of hierarchical porous Co_3O_4 microspheres and their application for electrochemical energy storage. *Electrochim. Acta* **2015**, *173*, 385–392. [CrossRef]
62. Yadav, A.A.; Hunge, Y.M.; Kulkarni, S.B. Chemical synthesis of Co_3O_4 nanowires for symmetric supercapacitor device. *J. Mater. Sci. Mater. El.* **2018**, *29*, 16401–16409. [CrossRef]
63. Chen, M.H.; Ge, Q.X.; Qi, M.L.; Liang, X.Q.; Wang, F.; Chen, Q.G. Cobalt oxides nanorods arrays as advanced electrode for high performance supercapacitor. *Surf. Coat. Technol.* **2019**, *360*, 73–77. [CrossRef]
64. Yao, M.; Hu, Z.; Xu, Z.; Liu, Y. Template synthesis of 1D hierarchical hollow Co_3O_4 nanotubes as high performance supercapacitor materials. *J. Alloys Compd.* **2015**, *644*, 721–728. [CrossRef]
65. Li, G.; Hua, X.; Liu, P.; Xie, Y.; Han, L. Porous Co_3O_4 microflowers prepared by thermolysis of metal-organic framework for supercapacitor. *Mater. Chem. Phys.* **2015**, *168*, 127–131. [CrossRef]
66. Xiao, Z.; Fan, L.; Xu, B.; Zhang, S.; Kang, W.; Kang, Z.; Lin, H.; Liu, X.; Zhang, S.; Sun, D. Green Fabrication of Ultrathin Co_3O_4 Nanosheets from Metal–Organic Framework for Robust High-Rate Supercapacitors. *ACS Appl. Mater. Interfaces* **2017**, *9*, 41827–41836. [CrossRef] [PubMed]
67. Wei, G.; Zhou, Z.; Zhao, X.; Zhang, W.; An, C. Ultrathin Metal–Organic Framework Nanosheet-Derived Ultrathin Co_3O_4 Nanomeshes with Robust Oxygen-Evolving Performance and Asymmetric Supercapacitors. *ACS Appl. Mater. Interfaces* **2018**, *10*, 23721–23730. [CrossRef]
68. Zhu, Z.; Han, C.; Li, T.-T.; Hu, Y.; Qian, J.; Huang, S. MOF-templated syntheses of porous Co_3O_4 hollow spheres and micro-flowers for enhanced performance in supercapacitors. *CrystEngComm* **2018**, *20*, 3812–3816. [CrossRef]
69. Yadav, A.A.; Chavan, U.J. Electrochemical supercapacitive performance of spray deposited Co_3O_4 thin film nanostructures. *Electrochim. Acta* **2017**, *232*, 370–376. [CrossRef]
70. Duan, Y.; Hu, T.; Yang, L.; Gao, J.; Guo, S.; Hou, M.; Ye, X. Facile fabrication of electroactive microporous Co_3O_4 through microwave plasma etching for supercapacitors. *J. Alloys Compd.* **2019**, *771*, 156–161. [CrossRef]
71. Kumar, M.; Subramania, A.; Balakrishnan, K. Preparation of electrospun Co_3O_4 nanofibers as electrode material for high performance asymmetric supercapacitors. *Electrochim. Acta* **2014**, *149*, 152–158. [CrossRef]
72. You, Y.; Zheng, M.; Ma, L.; Yuan, X.; Zhang, B.; Li, Q.; Wang, F.; Song, J.; Jiang, D.; Liu, P.; et al. Galvanic displacement assembly of ultrathin Co_3O_4 nanosheet arrays on nickel foam for a high-performance supercapacitor. *Nanotechnology* **2017**, *28*, 105604. [CrossRef]
73. Liu, X.Y.; Gao, Y.Q.; Yang, G.W. A flexible, transparent and super-long-life supercapacitor based on ultrafine Co_3O_4 nanocrystal electrodes. *Nanoscale* **2016**, *8*, 4227–4235. [CrossRef]
74. Jiang, T.; Yang, S.; Bai, Z.; Dai, P.; Yu, X.; Wu, M.; Hu, H. Facile fabrication and configuration design of Co_3O_4 porous acicular nanorod arrays on Ni foam for supercapacitors. *Nanotechnology* **2018**, *29*, 315402. [CrossRef] [PubMed]
75. Guan, C.; Qian, X.; Wang, X.H.; Cao, Y.Q.; Zhang, Q.; Li, A.D.; Wang, J. Atomic layer deposition of Co_3O_4 on carbon nanotubes/carbon cloth for high-capacitance and ultrastable supercapacitor electrode. *Nanotechnology* **2015**, *26*, 094001. [CrossRef] [PubMed]
76. Zhu, C.; Wang, M.; Li, T.; Lu, T.; Pan, L. In situ synthesis of porous Co_3O_4 polyhedra/carbon nanotubes heterostructures for highly efficient supercapacitors. *Ionics* **2017**, *23*, 2175–2183. [CrossRef]
77. Kazazi, M.; Sedighi, A.R.; Mokhtari, M.A. Pseudocapacitive performance of electrodeposited porous Co_3O_4 film on electrophoretically modified graphite electrodes with carbon nanotubes. *Appl. Surf. Sci.* **2018**, *441*, 251–257. [CrossRef]
78. Durukan, M.B.; Yuksel, R.; Unalan, H.E. Cobalt Oxide Nanoflakes on Single Walled Carbon Nanotube Thin Films for Supercapacitor Electrodes. *Electrochim. Acta* **2016**, *222*, 1475–1482. [CrossRef]
79. Zou, Y.; Cai, C.; Xiang, C.; Huang, P.; Chu, H.; She, Z.; Xu, F.; Sun, L.; Kraatz, H.-B. Simple synthesis of core-shell structure of Co–Co_3O_4@carbon-nanotube-incorporated nitrogen-doped carbon for high-performance supercapacitor. *Electrochim. Acta* **2018**, *261*, 537–547. [CrossRef]

80. Ramesh, S.; Haldorai, Y.; Sivasamy, A.; Kim, H.S. Nanostructured Co_3O_4/nitrogen doped carbon nanotube composites for high-performance supercapacitors. *Mater. Lett.* **2017**, *206*, 39–43. [CrossRef]
81. Liao, Q.; Wang, C. Amorphous FeOOH nanorods and Co_3O_4 nanoflakes as binder-free electrodes for high-performance all-solid-state asymmetric supercapacitors. *CrystEngComm* **2019**, *21*, 662–672. [CrossRef]
82. Agubra, V.A.; Zuniga, L.; Flores, D.; Villareal, J.; Alcoutlabi, M. Composite nanofibers as advanced materials for Li-ion, Li-O_2 and Li-S batteries. *Electrochim. Acta* **2016**, *192*, 529–550. [CrossRef]
83. Abouali, S.; Garakani, M.A.; Zhang, B.; Xu, Z.L.; Heidari, E.K.; Huang, J.Q.; Huang, J.; Kim, J.K. Electrospun Carbon Nanofibers with in Situ Encapsulated Co(3)O(4) Nanoparticles as Electrodes for High-Performance Supercapacitors. *ACS Appl. Mater. Interfaces* **2015**, *7*, 13503–13511. [CrossRef] [PubMed]
84. Sun, J.; Man, P.; Zhang, Q.; He, B.; Zhou, Z.; Li, C.; Wang, X.; Guo, J.; Zhao, J.; Xie, L.; et al. Hierarchically-structured Co_3O_4 nanowire arrays grown on carbon nanotube fibers as novel cathodes for high-performance wearable fiber-shaped asymmetric supercapacitors. *Appl. Surf. Sci.* **2018**, *447*, 795–801. [CrossRef]
85. Shi, Z.; Xing, L.; Liu, Y.; Gao, Y.; Liu, J. A porous biomass-based sandwich-structured Co_3O_4@Carbon Fiber@Co_3O_4 composite for high-performance supercapacitors. *Carbon* **2018**, *129*, 819–825. [CrossRef]
86. Chen, M.H.; Chen, S.; Qi, M.L.; Zhang, J.W.; Yin, J.H.; Chen, Q.G.; Xia, X.H. Carbon cloth/cobalt oxide integrated electrode as flexible cathode of alkaline batteries. *Mater. Technol.* **2016**, *31*, 492–496. [CrossRef]
87. Aldama, I.; Barranco, V.; Centeno, T.A.; Ibanez, J.; Rojo, J.M. Composite Electrodes Made from Carbon Cloth as Supercapacitor Material and Manganese and Cobalt Oxide as Battery One. *J. Electrochem. Soc.* **2016**, *163*, 758–765. [CrossRef]
88. Balasubramanian, S.; Kamatchi Kamaraj, P. Fabrication of Natural Polymer Assisted Mesoporous Co_3O_4/Carbon Composites for Supercapacitors. *Electrochim. Acta* **2015**, *168*, 50–58. [CrossRef]
89. Zhou, S.S.; Ye, Z.C.; Hu, S.Z.; Hao, C.; Wang, X.H.; Huang, C.X.; Wu, F.S. Designed formation of Co_3O_4/$ZnCo_2O_4$/CuO hollow polyhedral nanocages derived from zeolitic imidazolate framework-67 for high-performance supercapacitors. *Nanoscale* **2018**, *10*, 15771–15781. [CrossRef]
90. Hao, S.J.; Zhang, B.W.; Wang, Y.; Li, C.J.; Feng, J.Y.; Ball, S.; Srinivasan, M.; Wu, J.S.; Huang, Y.Z. Hierarchical three-dimensional Fe_3O_4@porous carbon matrix/graphene anodes for high performance lithium ion batteries. *Electrochim. Acta* **2018**, *260*, 965–973. [CrossRef]
91. Zhou, F.Y.; Liu, Q.L.; Gu, J.J.; Zhang, W.; Zhang, D. A facile low-temperature synthesis of highly distributed and size-tunable cobalt oxide nanoparticles anchored on activated carbon for supercapacitors. *J. Power Sources* **2015**, *273*, 945–953. [CrossRef]
92. Wang, N.; Liu, Q.; Kang, D.; Gu, J.; Zhang, W.; Zhang, D. Facile Self-Cross-Linking Synthesis of 3D Nanoporous Co_3O_4/Carbon Hybrid Electrode Materials for Supercapacitors. *ACS Appl. Mater. Interfaces* **2016**, *8*, 16035–16044. [CrossRef]
93. Xu, Z.M.; Younis, A.; Chu, D.W.; Ao, Z.M.; Xu, H.L.; Li, S.A. Electrodeposition of Mesoporous Co_3O_4 Nanosheets on Carbon Foam for High Performance Supercapacitors. *J. Nanomater.* **2014**, *2014*, 5. [CrossRef]
94. Li, X.; Li, X.; Dong, Y.; Wang, L.; Jin, C.; Zhou, N.; Chen, M.; Dong, Y.; Xie, Z.; Zhang, C. Porous cobalt oxides/carbon foam hybrid materials for high supercapacitive performance. *J. Colloid Interface Sci.* **2019**, *542*, 102–111. [CrossRef] [PubMed]
95. Kim, M.; Oh, I.; Ju, H.; Kim, J. Introduction of Co_3O_4 into activated honeycomb-like carbon for the fabrication of high performance electrode materials for supercapacitors. *Phys. Chem. Chem. Phys.* **2016**, *18*, 9124–9132. [CrossRef] [PubMed]
96. Haldorai, Y.; Choe, S.R.; Huh, Y.S.; Han, Y.K. Metal-organic framework derived nanoporous carbon/Co_3O_4 composite electrode as a sensing platform for the determination of glucose and high-performance supercapacitor. *Carbon* **2018**, *127*, 366–373. [CrossRef]
97. Zhang, G.X.; Chen, Y.M.; Jiang, Y.J.; Lin, C.; Chen, Y.G.; Guo, H.B. Formation of CMK-3/Co_3O_4 nanosheets on nickel foam with markedly enhanced pseudocapacitive properties. *J. Mater. Sci. Technol.* **2018**, *34*, 1538–1543. [CrossRef]
98. Hu, P.D.; Long, M.C.; Bai, X.; Wang, C.; Cai, C.Y.; Fu, J.J.; Zhou, B.X.; Zhou, Y.F. Monolithic cobalt-doped carbon aerogel for efficient catalytic activation of peroxymonosulfate in water. *J. Hazard. Mater.* **2017**, *332*, 195–204. [CrossRef]

99. Esfahani, M.Z.; Aghaei, A.; Khosravi, M.; Bagheri, N.; Khakpoura, Z.; Javaheri, M. Pore structure improvement of carbon aerogel and investigation of the supercapacitive behavior of a Co_3O_4 nanoball/carbon aerogel composite. *New J. Chem.* **2017**, *41*, 11731–11741. [CrossRef]
100. Sun, G.L.; Ma, L.Y.; Ran, J.B.; Shen, X.Y.; Tong, H. Incorporation of homogeneous Co_3O_4 into a nitrogen-doped carbon aerogel via a facile in situ synthesis method: Implications for high performance asymmetric supercapacitors. *J. Mater. Chem. A* **2016**, *4*, 9542–9554. [CrossRef]
101. Cui, J.F.; Xi, Y.L.; Chen, S.; Li, D.H.; She, X.L.; Sun, J.; Han, W.; Yang, D.J.; Guo, S.J. Prolifera-Green-Tide as Sustainable Source for Carbonaceous Aerogels with Hierarchical Pore to Achieve Multiple Energy Storage. *Adv. Funct. Mater.* **2016**, *26*, 8487–8495. [CrossRef]
102. Zhang, H.; Zhou, Y.Y.; Ma, Y.B.; Yao, J.R.; Li, X.; Sun, Y.Y.; Xiong, Z.Y.; Li, D. RF magnetron sputtering synthesis of three-dimensional graphene@Co_3O_4 nanowire array grown on Ni foam for application in supercapacitors. *J. Alloys Compd.* **2018**, *740*, 174–179. [CrossRef]
103. Yang, S.; Liu, Y.; Hao, Y.; Yang, X.; Goddard, W.A., 3rd; Zhang, X.L.; Cao, B. Oxygen-Vacancy Abundant Ultrafine Co_3O_4/Graphene Composites for High-Rate Supercapacitor Electrodes. *Adv. Sci.* **2018**, *5*, 1700659. [CrossRef] [PubMed]
104. Tian, X.; Sun, X.; Jiang, Z.; Jiang, Z.-J.; Hao, X.; Shao, D.; Maiyalagan, T. Exploration of the Active Center Structure of Nitrogen-Doped Graphene for Control over the Growth of Co_3O_4 for a High-Performance Supercapacitor. *ACS Appl. Energy Mater.* **2018**, *1*, 143–153. [CrossRef]
105. Hu, Y.; Guan, C.; Feng, G.; Ke, Q.; Huang, X.; Wang, J. Flexible Asymmetric Supercapacitor Based on Structure-Optimized Mn3O4/Reduced Graphene Oxide Nanohybrid Paper with High Energy and Power Density. *Adv. Funct. Mater.* **2015**, *25*, 7291–7299. [CrossRef]
106. Tan, H.Y.; Yu, B.Z.; Cao, L.L.; Cheng, T.; Zheng, X.L.; Li, X.H.; Li, W.L.; Ren, Z.Y. Layer-dependent growth of two-dimensional Co_3O_4 nanostructure arrays on graphene for high performance supercapacitors. *J. Alloys Compd.* **2017**, *696*, 1180–1188. [CrossRef]
107. Yin, D.; Huang, G.; Sun, Q.; Li, Q.; Wang, X.; Yuan, D.; Wang, C.; Wang, L. RGO/Co_3O_4 Composites Prepared Using GO-MOFs as Precursor for Advanced Lithium-ion Batteries and Supercapacitors Electrodes. *Electrochim. Acta* **2016**, *215*, 410–419. [CrossRef]
108. Lai, C.; Sun, Y.; Zhang, X.; Yang, H.; Lin, B. High-performance double ion-buffering reservoirs of asymmetric supercapacitors based on flower-like Co_3O_4-G>N-PEGm microspheres and 3D rGO-CNT>N-PEGm aerogels. *Nanoscale* **2018**, *10*, 17293–17303. [CrossRef] [PubMed]
109. Wang, X.; Wu, D.; Song, X.; Du, W.; Zhao, X.; Zhang, D. Review on Carbon/Polyaniline Hybrids: Design and Synthesis for Supercapacitor. *Molecules* **2019**, *24*, 2263. [CrossRef]
110. Xu, J.; Xiao, T.; Tan, X.; Xiang, P.; Jiang, L.; Wu, D.; Li, J.; Wang, S. A new asymmetric aqueous supercapacitor: Co_3O_4//Co_3O_4@polypyrrole. *J. Alloys Compd.* **2017**, *706*, 351–357. [CrossRef]
111. Qi, M.; Xie, D.; Zhong, Y.; Chen, M.; Xia, X. Smart construction of polyaniline shell on cobalt oxides as integrated core-shell arrays for enhanced lithium ion batteries. *Electrochim. Acta* **2017**, *247*, 701–707. [CrossRef]
112. Mai, Y.J.; Xia, X.H.; Jie, X.H. Conformal construction of polyaniline shell on cobalt oxide nanoflake core for enhanced Li ion storage. *Mater. Res. Bull.* **2017**, *94*, 216–221. [CrossRef]
113. Hai, Z.; Gao, L.; Zhang, Q.; Xu, H.; Cui, D.; Zhang, Z.; Tsoukalas, D.; Tang, J.; Yan, S.; Xue, C. Facile synthesis of core–shell structured PANI-Co_3O_4 nanocomposites with superior electrochemical performance in supercapacitors. *Appl. Surf. Sci.* **2016**, *361*, 57–62. [CrossRef]
114. Ren, X.; Fan, H.; Ma, J.; Wang, C.; Zhang, M.; Zhao, N. Hierarchical Co_3O_4/PANI hollow nanocages: Synthesis and application for electrode materials of supercapacitors. *Appl. Surf. Sci.* **2018**, *441*, 194–203. [CrossRef]
115. Padwal, P.M.; Kadam, S.L.; Mane, S.M.; Kulkarni, S.B. Synthesis and characterization of supercapacitive behavior of electrodeposited PANI/Co_3O_4 layered composite electrode. *J. Chin. Chem. Soc. Taip.* **2016**, *4*, 13–23.
116. Yang, X.; Xu, K.; Zou, R.; Hu, J. A Hybrid Electrode of Co_3O_4@PPy Core/Shell Nanosheet Arrays for High-Performance Supercapacitors. *Nanomicro. Lett.* **2016**, *8*, 143–150. [CrossRef]
117. Huang, Y.; Li, H.; Wang, Z.; Zhu, M.; Pei, Z.; Xue, Q.; Huang, Y.; Zhi, C. Nanostructured Polypyrrole as a flexible electrode material of supercapacitor. *Nano Energy* **2016**, *22*, 422–438. [CrossRef]
118. Guo, D.; Zhang, M.; Chen, Z.; Liu, X. Hierarchical Co_3O_4@PPy core-shell composite nanowires for supercapacitors with enhanced electrochemical performance. *Mater. Res. Bull.* **2017**, *96*, 463–470. [CrossRef]

119. Wu, X.; Meng, L.; Wang, Q.; Zhang, W.; Wang, Y. A flexible asymmetric fibered-supercapacitor based on unique Co_3O_4@PPy core-shell nanorod arrays electrode. *Chem. Eng. J.* **2017**, *327*, 193–201. [CrossRef]
120. Ma, L.T.; Fan, H.Q.; Wei, X.Y.; Chen, S.M.; Hu, Q.Z.; Liu, Y.; Zhi, C.Y.; Lu, W.; Zapien, J.A.; Huang, H.T. Towards high areal capacitance, rate capability, and tailorable supercapacitors: Co_3O_4@polypyrrole core-shell nanorod bundle array electrodes. *J. Mater. Chem. A* **2018**, *6*, 19058–19065. [CrossRef]
121. Ozkazanc, E. PTh/Co_3O_4 nanocomposites as new conducting materials for micro/nano-sized electronic devices. *Polym. Eng. Sci.* **2017**, *57*, 1168–1178.
122. Reddy, B.N.; Deshagani, S.; Deepa, M.; Ghosal, P. Effective pseudocapacitive charge storage/release by hybrids of poly(3,4-ethylenedioxypyrrole) with Fe_3O_4 nanostructures or Co_3O_4 nanorods. *Chem. Eng. J.* **2018**, *334*, 1328–1340. [CrossRef]
123. Raj, R.P.; Ragupathy, P.; Mohan, S. Remarkable capacitive behavior of a Co_3O_4–polyindole composite as electrode material for supercapacitor applications. *J. Mater. Chem. A* **2015**, *3*, 24338–24348. [CrossRef]
124. Pang, M.; Long, G.; Jiang, S.; Ji, Y.; Han, W.; Wang, B.; Liu, X.; Xi, Y.; Wang, D.; Xu, F. Ethanol-assisted solvothermal synthesis of porous nanostructured cobalt oxides (CoO/Co_3O_4) for high-performance supercapacitors. *Chem. Eng. J.* **2015**, *280*, 377–384. [CrossRef]
125. Hu, Q.; Gu, Z.; Zheng, X.; Zhang, X. Three-dimensional Co_3O_4@NiO hierarchical nanowire arrays for solid-state symmetric supercapacitor with enhanced electrochemical performances. *Chem. Eng. J.* **2016**, *304*, 223–231. [CrossRef]
126. Ambare, R.C.; Bharadwaj, S.R.; Lokhande, B.J. Non-aqueous route spray pyrolyzed Ru:Co_3O_4 thin electrodes for supercapacitor application. *Appl. Surf. Sci.* **2015**, *349*, 887–896. [CrossRef]
127. Feng, M.; Zhang, G.; Du, Q.; Su, L.; Ma, Z.; Qin, X.; Shao, G. Co_3O_4@MnO_2 core shell arrays on nickel foam with excellent electrochemical performance for aqueous asymmetric supercapacitor. *Ionics* **2017**, *23*, 1637–1643. [CrossRef]
128. Wang, K.; Shi, Z.; Wang, Y.; Ye, Z.; Xia, H.; Liu, G.; Qiao, G. Co_3O_4 nanowires@MnO_2 nanolayer or nanoflakes core–shell arrays for high-performance supercapacitors: The influence of morphology on performance. *J. Alloys Compd.* **2015**, *624*, 85–93. [CrossRef]
129. Xing, L.; Dong, Y.; Hu, F.; Wu, X.; Umar, A. Co_3O_4 nanowire@NiO nanosheet arrays for high performance asymmetric supercapacitors. *Dalton T.* **2018**, *47*, 5687–5694. [CrossRef]
130. Yang, F.; Xu, K.; Hu, J. Construction of Co_3O_4@Fe_2O_3 core-shell nanowire arrays electrode for supercapacitors. *J. Alloys Compd.* **2017**, *729*, 1172–1176. [CrossRef]
131. Chandra Sekhar, S.; Nagaraju, G.; Yu, J.S. High-performance pouch-type hybrid supercapacitor based on hierarchical NiO-Co_3O_4-NiO composite nanoarchitectures as an advanced electrode material. *Nano Energy* **2018**, *48*, 81–92. [CrossRef]
132. Hu, N.; Gong, W.H.; Huang, L.; Shen, P.K. Ultrahigh energy density asymmetric electrochemical capacitors based on flower-like ZnO/Co_3O_4 nanobundle arrays and stereotaxically constricted graphene. *J. Mater. Chem. A* **2019**, *7*, 1273–1280. [CrossRef]
133. Harilal, M.; Vidyadharan, B.; Misnon, I.I.; Anilkumar, G.M.; Lowe, A.; Ismail, J.; Yusoff, M.M.; Jose, R. One-Dimensional Assembly of Conductive and Capacitive Metal Oxide Electrodes for High-Performance Asymmetric Supercapacitors. *ACS Appl. Mater. Interfaces* **2017**, *9*, 10730–10742. [CrossRef] [PubMed]
134. Cheng, M.; Duan, S.; Fan, H.; Su, X.; Cui, Y.; Wang, R. Core@shell CoO@Co_3O_4 nanocrystals assembling mesoporous microspheres for high performance asymmetric supercapacitors. *Chem. Eng. J.* **2017**, *327*, 100–108. [CrossRef]
135. Jinlong, L.; Meng, Y.; Tongxiang, L.; Miura, H. Facile synthesis of Co_3O_4@MnO_2 core–shell nanocomposites for high-performance supercapacitor. *Mater. Lett.* **2017**, *197*, 127–130. [CrossRef]
136. Du, G.J.; Liu, X.G.; Zong, Y.; Hor, T.S.A.; Yu, A.S.; Liu, Z.L. Co_3O_4 nanoparticle-modified MnO_2 nanotube bifunctional oxygen cathode catalysts for rechargeable zinc-air batteries. *Nanoscale* **2013**, *5*, 4657–4661. [CrossRef] [PubMed]
137. Chen, H.Y.; Wang, J.P.; Liao, F.; Han, X.R.; Xu, C.J.; Zhang, Y.F. Facile synthesis of porous Mn-doped Co_3O_4 oblique prisms as an electrode material with remarkable pseudocapacitance. *Ceram. Int.* **2019**, *45*, 8008–8016. [CrossRef]
138. Zhang, C.; Wei, J.; Chen, L.; Tang, S.; Deng, M.; Du, Y. All-solid-state asymmetric supercapacitors based on Fe-doped mesoporous Co_3O_4 and three-dimensional reduced graphene oxide electrodes with high energy and power densities. *Nanoscale* **2017**, *9*, 15423–15433. [CrossRef]

139. Deng, S.; Xiao, X.; Chen, G.; Wang, L.; Wang, Y. Cd doped porous Co_3O_4 nanosheets as electrode material for high performance supercapacitor application. *Electrochim. Acta* **2016**, *196*, 316–327. [CrossRef]
140. Li, G.M.; Chen, M.Z.; Ouyang, Y.; Yao, D.; Li, L.; Wang, L.; Xia, X.F.; Lei, W.; Chen, S.M.; Mandler, D.; et al. Manganese doped Co_3O_4 mesoporous nanoneedle array for long cycle-stable supercapacitors. *Appl. Surf. Sci.* **2019**, *469*, 941–950. [CrossRef]
141. Krishnan, S.G.; Reddy, M.V.; Harilal, M.; Vidyadharan, B.; Misnon, I.I.; Rahim, M.H.A.; Ismail, J.; Jose, R. Characterization of $MgCo_2O_4$ as an electrode for high performance supercapacitors. *Electrochim. Acta* **2015**, *161*, 312–321. [CrossRef]
142. Vadiyar, M.M.; Kolekar, S.S.; Chang, J.-Y.; Kashale, A.A.; Ghule, A.V. Reflux Condensation Mediated Deposition of Co_3O_4 Nanosheets and $ZnFe_2O_4$ Nanoflakes Electrodes for Flexible Asymmetric Supercapacitor. *Electrochim. Acta* **2016**, *222*, 1604–1615. [CrossRef]
143. Zhao, L.G.; Yang, M.; Zhang, Z.Q.; Ji, Y.; Teng, Y.F.; Feng, Y.; Liu, X.Y. Hierarchical micro/nanostructured Co_3O_4@$MnCo_2O_4$ core-shell nanowire arrays on Ni foam for electrochemical energy storage. *Inorg. Chem. Commun.* **2018**, *89*, 22–26. [CrossRef]
144. Dong, B.; Zhang, X.; Xu, X.; Gao, G.; Ding, S.; Li, J.; Li, B. Preparation of scale-like nickel cobaltite nanosheets assembled on nitrogen-doped reduced graphene oxide for high-performance supercapacitors. *Carbon* **2014**, *80*, 222–228. [CrossRef]
145. Wang, W.; Yang, Y.; Yang, S.; Guo, Z.; Feng, C.; Tang, X. Synthesis and electrochemical performance of ZnCo2O4 for lithium-ion battery application. *Electrochim. Acta* **2015**, *155*, 297–304. [CrossRef]
146. Sennu, P.; Aravindan, V.; Lee, Y.S. High energy asymmetric supercapacitor with 1D@2D structured $NiCo_2O_4$@Co_3O_4 and jackfruit derived high surface area porous carbon. *J. Power Sources* **2016**, *306*, 248–257. [CrossRef]
147. Zhang, M.; Fan, H.; Zhao, N.; Peng, H.; Ren, X.; Wang, W.; Li, H.; Chen, G.; Zhu, Y.; Jiang, X.; et al. 3D hierarchical $CoWO_4$/Co_3O_4 nanowire arrays for asymmetric supercapacitors with high energy density. *Chem. Eng. J.* **2018**, *347*, 291–300. [CrossRef]
148. Cui, S.X.; Li, T.T.; Guo, C.L.; Wang, L.L.; Zhang, C.C.; Yan, Z.Y.; Wei, Y.H.; Hou, L.F.; Xu, L.C.; Jia, C.K. Synthesis of Mesoporous Co_3O_4/$NiCo_2O_4$ Nanorods and Their Electrochemical Study. *J Nanosci. Nanotechno.* **2019**, *19*, 47–56. [CrossRef]
149. Yang, F.; Xu, K.B.; Hu, J.Q. Hierarchical multicomponent electrode with $NiMoO_4$ nanosheets coated on Co_3O_4 nanowire arrays for enhanced electrochemical properties. *J. Alloys Compd.* **2019**, *781*, 1127–1131. [CrossRef]
150. Xu, K.; Yang, X.; Yang, J.; Hu, J. Synthesis of hierarchical Co_3O_4@$NiCo_2O_4$ core-shell nanosheets as electrode materials for supercapacitor application. *J. Alloys Compd.* **2017**, *700*, 247–251. [CrossRef]
151. Dong, T.; Li, M.; Wang, P.; Yang, P. Synthesis of hierarchical tube-like yolk-shell Co_3O_4@$NiMoO_4$ for enhanced supercapacitor performance. *Int. J. Hydrogen Energy* **2018**, *43*, 14569–14577. [CrossRef]
152. Zhang, M.C.; Fan, H.Q.; Ren, X.H.; Zhao, N.; Peng, H.J.; Wang, C.; Wu, X.B.; Dong, G.Z.; Long, C.B.; Wang, W.J.; et al. Study of pseudocapacitive contribution to superior energy storage of 3D heterostructure $CoWO_4$/Co_3O_4 nanocone arrays. *J. Power Sources* **2019**, *418*, 202–210. [CrossRef]
153. Hu, X.W.; Liu, S.; Qu, B.T.; You, X.Z. Starfish-shaped Co_3O_4/$ZnFe_2O_4$ Hollow Nanocomposite: Synthesis, Supercapacity, and Magnetic Properties. *ACS Appl. Mater. Interfaces* **2015**, *7*, 9972–9981. [CrossRef] [PubMed]
154. Sapna; Budhiraja, N.; Kumar, V.; Singh, S.K. Synergistic effect in structural and supercapacitor performance of well dispersed $CoFe_2O_4$/Co_3O_4 nano-hetrostructures. *Ceram. Int.* **2018**, *44*, 13806–13814. [CrossRef]
155. Chen, X.B.; Liu, X.; Liu, Y.X.; Zhu, Y.M.; Zhuang, G.C.; Zheng, W.; Cai, Z.Y.; Yang, P.Z. Advanced binder-free electrodes based on $CoMn_2O_4$@Co_3O_4 core/shell nanostructures for high-performance supercapacitors. *RSC Adv.* **2018**, *8*, 31594–31602. [CrossRef]
156. Zhou, J.-J.; Han, X.; Tao, K.; Li, Q.; Li, Y.-L.; Chen, C.; Han, L. Shish-kebab type $MnCo_2O_4$@Co_3O_4 nanoneedle arrays derived from MnCo-LDH@ZIF-67 for high-performance supercapacitors and efficient oxygen evolution reaction. *Chem. Eng. J.* **2018**, *354*, 875–884. [CrossRef]
157. Liu, X.; Zhou, A.; Pan, T.; Dou, Y.; Shao, M.; Han, J.; Wei, M. Ultrahigh-rate-capability of a layered double hydroxide supercapacitor based on a self-generated electrolyte reservoir. *J. Mater. Chem. A* **2016**, *4*, 8421–8427. [CrossRef]

158. Qorbani, M.; Naseri, N.; Moshfegh, A.Z. Hierarchical Co_3O_4/$Co(OH)_2$ Nanoflakes as a Supercapacitor Electrode: Experimental and Semi-Empirical Model. *ACS Appl. Mater. Interfaces* **2015**, *7*, 11172–11179. [CrossRef]
159. Pan, X.X.; Ji, F.Z.; Kuang, L.P.; Liu, F.; Zhang, Y.; Chen, X.M.; Alameh, K.; Ding, B.F. Synergetic Effect of Three-Dimensional Co_3O_4@$Co(OH)_2$ Hybrid Nanostructure for Electrochemical Energy Storage. *Electrochim. Acta* **2016**, *215*, 298–304. [CrossRef]
160. Bai, X.; Liu, Q.; Liu, J.; Zhang, H.; Li, Z.; Jing, X.; Liu, P.; Wang, J.; Li, R. Hierarchical Co_3O_4@$Ni(OH)_2$ core-shell nanosheet arrays for isolated all-solid state supercapacitor electrodes with superior electrochemical performance. *Chem. Eng. J.* **2017**, *315*, 35–45. [CrossRef]
161. Su, D.; Tang, Z.; Xie, J.; Bian, Z.; Zhang, J.; Yang, D.; Zhang, D.; Wang, J.; Liu, Y.; Yuan, A.; et al. Co, Mn-LDH nanoneedle arrays grown on Ni foam for high performance supercapacitors. *Appl. Surf. Sci.* **2019**, *469*, 487–494. [CrossRef]
162. Zhou, J.J.; Li, Q.; Chen, C.; Li, Y.L.; Tao, K.; Han, L. Co_3O_4@CoNi-LDHcore/shell nanosheet arrays for high-performance battery-type supercapacitors. *Chem. Eng. J.* **2018**, *350*, 551–558. [CrossRef]
163. Quan, W.; Xu, Y.; Wang, Y.; Meng, S.; Jiang, D.; Chen, M. Hierarchically structured Co_3O_4@glucose-modified LDH architectures for high-performance supercapacitors. *Appl. Surf. Sci.* **2019**, *488*, 639–647. [CrossRef]
164. Li, X.; Yang, Z.C.; Qi, W.; Li, Y.T.; Wu, Y.; Zhou, S.X.; Huang, S.M.; Wei, J.; Li, H.J.; Yao, P. Binder-free Co_3O_4@NiCoAl-layered double hydroxide core-shell hybrid architectural nanowire arrays with enhanced electrochemical performance. *Appl. Surf. Sci.* **2016**, *363*, 381–388. [CrossRef]
165. Chen, J.S.; Guan, C.; Gui, Y.; Blackwood, D.J. Rational Design of Self-Supported Ni_3S_2 Nanosheets Array for Advanced Asymmetric Supercapacitor with a Superior Energy Density. *ACS Appl. Mater. Interfaces* **2017**, *9*, 496–504. [CrossRef] [PubMed]
166. Ning, J.; Zhang, T.; He, Y.; Jia, C.; Saha, P.; Cheng, Q. Co_3O_4@CoS core-shell nanosheets on carbon cloth for high performance supercapacitor electrodes. *Materials* **2017**, *10*, 608. [CrossRef] [PubMed]
167. Yan, Y.; Li, K.; Chen, X.; Yang, Y.; Lee, J.-M. Heterojunction-Assisted Co_3S_4@Co_3O_4 Core–Shell Octahedrons for Supercapacitors and Both Oxygen and Carbon Dioxide Reduction Reactions. *Small* **2017**, *13*, 1701724. [CrossRef] [PubMed]
168. Zhang, J.; Lin, J.; Wu, J.; Xu, R.; Lai, M.; Gong, C.; Chen, X.; Zhou, P. Excellent Electrochemical Performance Hierarchical Co_3O_4@Ni_3S_2 core/shell nanowire arrays for Asymmetric Supercapacitors. *Electrochim. Acta* **2016**, *207*, 87–96. [CrossRef]
169. Patil, D.S.; Pawar, S.A.; Shin, J.C. Core-shell structure of Co_3O_4@CdS for high performance electrochemical supercapacitor. *Chem. Eng. J.* **2018**, *335*, 693–702. [CrossRef]
170. Pawar, S.A.; Patil, D.S.; Shin, J.C. Designing a Copper- and Silver-Sulfide Composite with Co_3O_4 for High-Performance Electrochemical Supercapacitors. *Chemelectrochem* **2019**, *6*, 522–534. [CrossRef]
171. Feng, X.S.; Huang, Y.; Li, C.; Chen, X.F.; Zhou, S.H.; Gao, X.G.; Chen, C. Controllable synthesis of porous $NiCo_2O_4$/NiO/Co_3O_4 nanoflowers for asymmetric all-solid-state supercapacitors. *Chem. Eng. J.* **2019**, *368*, 51–60. [CrossRef]
172. Zhao, J.; Li, Y.; Xu, Z.; Wang, D.; Ban, C.; Zhang, H. Unique porous Mn_2O_3/C cube decorated by Co_3O_4 nanoparticle: Low-cost and high-performance electrode materials for asymmetric supercapacitors. *Electrochim. Acta* **2018**, *289*, 72–81. [CrossRef]
173. Zhang, M.; Wang, C.H.; Liu, C.; Luo, R.; Li, J.S.; Sun, X.Y.; Shen, J.Y.; Han, W.Q.; Wang, L.J. Metal-organic framework derived Co_3O_4/C@SiO_2 yolk-shell nanoreactors with enhanced catalytic performance. *J. Mater. Chem. A* **2018**, *6*, 11226–11235. [CrossRef]
174. Dai, S.; Yuan, Y.; Yu, J.; Tang, J.; Zhou, J.; Tang, W. Metal-organic framework-templated synthesis of sulfur-doped core-sheath nanoarrays and nanoporous carbon for flexible all-solid-state asymmetric supercapacitors. *Nanoscale* **2018**, *10*, 15454–15461. [CrossRef] [PubMed]
175. Abidin, S.; Mamat, M.S.; Rasyid, S.A.; Zainal, Z.; Sulaiman, Y. Electropolymerization of poly(3,4-ethylenedioxythiophene) onto polyvinyl alcohol-graphene quantum dot-cobalt oxide nanofiber composite for high-performance supercapacitor. *Electrochim. Acta* **2018**, *261*, 548–556. [CrossRef]
176. Li, S.T.; Duan, Y.A.; Teng, Y.; Fan, N.; Huo, Y.Q. MOF-derived tremelliform Co_3O_4/NiO/Mn_2O_3 with excellent capacitive performance. *Appl. Surf. Sci.* **2019**, *478*, 247–254. [CrossRef]

177. Zhou, S.S.; Hao, C.; Wang, J.J.; Wang, X.H.; Gao, H.W. Metal-organic framework templated synthesis of porous $NiCo_2O_4$/$ZnCo_2O_4$/Co_3O_4 hollow polyhedral nanocages and their enhanced pseudocapacitive properties. *Chem. Eng. J.* **2018**, *351*, 74–84. [CrossRef]
178. Wang, Y.; Lu, Y.; Chen, K.; Cui, S.; Chen, W.; Mi, L. Synergistic effect of Co_3O_4@C@MnO_2 nanowire heterostructures for high-performance asymmetry supercapacitor with long cycle life. *Electrochim. Acta* **2018**, *283*, 1087–1094. [CrossRef]
179. Su, F.; Lyu, X.; Liu, C.; Miao, M. Flexible two-ply yarn supercapacitors based on carbon nanotube/stainless steel core spun yarns decorated with Co_3O_4 nanoparticles and MnOx composites. *Electrochim. Acta* **2016**, *215*, 535–542. [CrossRef]
180. Jiang, L.L.; Li, Y.J.; Luo, D.; Zhang, Q.Y.; Cai, F.G.; Wan, G.J.; Xiong, L.; Ren, Z.F. Freestanding RGO-Co_3O_4-PPy Composite Films as Electrodes for Supercapacitors. *Energy Tecnol.* **2019**, *7*, 1800606. [CrossRef]
181. Yan, S.; Xu, L.N.; Jiang, J.; Xiao, H.P.; Li, X.H. An extra-long-life supercapacitor based on Co_3O_4/$NiCo_2O_4$/NiO/C&S composite by decomposition of Co/Ni-based coordination complex. *J. Alloys Compd.* **2018**, *764*, 684–690.